AN OVERVIEW OF THE THEORY OF LOWER HYBRID AND ION CYCLOTRON HEATING OF TOKAMAK PLASMAS

Marco Bambilla

IPP 5/20 June 1988

MAX-PLANCK-INSTITUT FÜR PLASMAPHYSIK

8046 GARCHING BEI MÜNCHEN

MAX-PLANCK-INSTITUT FÜR PLASMAPHYSIK
GARCHING BEI MÜNCHEN

AN OVERVIEW OF THE THEORY OF LOWER HYBRID AND ION CYCLOTRON HEATING OF TOKAMAK PLASMAS

Marco Bambilla

IPP 5/20 June 1988

Die nachstehende Arbeit wurde im Rahmen des Vertrages zwischen dem Max-Planck-Institut für Plasmaphysik und der Europäischen Atomgemeinschaft über die Zusammenarbeit auf dem Gebiete der Plasmaphysik durchgeführt.

AN OVERVIEW OF THE THEORY OF LOWER HYBRID AND ION CYCLOTRON HEATING OF TOKAMAK PLASMAS

MARCO BRAMBILLA

Max-Planck Institute für Plasmaphysik - Euratom Association
Garching bei München, W. Germany

ABSTRACT

These notes are an introduction to the theory of Lower Hybrid Resonance (LHR) and Ion Cyclotron Resonance (ICR) heating of Tokamak plasmas. This choice does not imply that other HF heating methods, particularly Electron Cyclotron Resonance (ECR) and Alfvén Wave Resonance (AWR) heating, are less interesting: it just takes into account the competences of the author.

Even within this restricted scope, it was of course not possible to cover even superficially all the topics of interest. We have devoted some effort to discuss the linear dispersion relation and the mechanisms of wave–particle interactions, since we are convinced that a good understanding of linear propagation and absorption is a pre–requisite for any deeper investigation of h.f. plasma heating. In particular we have tried to show how the guidelines for heating experiments (frequency choice, antenna design, etc.), are dictated by the properties of linear plasma waves. A cursory mention has been given of other subjects of obvious importance: solution of Maxwell equations in non–uniform plasmas, antenna modeling, h.f. current drive. Practically nothing is said on parametric decay processes, h.f. effects on confinement and impurity production, etc..

I would like to thank the organisators of the 3d Latin–American Workshop in Plasma Physics for the invitation to give these lectures, and for the generous financial support which has made possible my participation to the meeting.

1 - THE DISPERSION RELATION OF LOW FREQUENCY WAVES.

1.1 - The dispersion relation. The linear response of a uniform plasma to a plane wave of frequency ω and wavevector $\vec{k}$ (of the form $\vec{E} = \vec{E}_0 e^{i(\vec{k}\cdot\vec{r}-\omega t)}$) is completely described by the dielectric tensor $\underline{\underline{\epsilon}}(\vec{k},\omega)$, defined through:

$$\vec{D} = \vec{E} + \frac{4\pi i}{\omega}\vec{J} = \underline{\underline{\epsilon}} \cdot \vec{E} \tag{1.1}$$

The reader can find the derivation of $\underline{\underline{\epsilon}}$ by integration of the linearised Vlasov equation along the unperturbed particle orbits in [1]. For a plasma with Maxwellian distribution functions, this leads to:

$$\begin{aligned}
\epsilon_{xx} &= 1 - \sum_j \frac{\omega_{pj}}{\omega^2} \sum_{n=-\infty}^{+\infty} \frac{n^2}{\lambda_j} I_n(\lambda_j) e^{-\lambda_j} \left(-x_{0j} Z(x_{nj})\right) \\
\epsilon_{xy} &= -\epsilon_{yx} = i \sum_j \frac{\omega_{pj}}{\omega^2} \sum_{n=-\infty}^{+\infty} n \left[I_n(\lambda_j) - I_n'(\lambda_j)\right] e^{-\lambda_j} \left(-x_{0j} Z(x_{nj})\right) \\
\epsilon_{xz} &= \epsilon_{zx} = -\frac{1}{2} n_\perp n_\parallel \sum_j \frac{\omega_{pj}^2}{\omega \Omega_j} \frac{v_{thj}^2}{c^2} \sum_{n=-\infty}^{+\infty} \frac{n}{\lambda_j} I_n(\lambda_j) e^{-\lambda_j} x_{0j}^2 Z'(x_{nj}) \\
\epsilon_{yy} &= 1 - \sum_j \frac{\omega_{pj}}{\omega^2} \sum_{n=-\infty}^{+\infty} \left\{ \frac{n^2}{\lambda_j} I_n(\lambda_j) + 2\lambda_j \left[I_n(\lambda_j) - I_n'(\lambda_j)\right] \right\} e^{-\lambda_j} \left(-x_{0j} Z(x_{nj})\right) \\
\epsilon_{yz} &= -\epsilon_{zy} = -\frac{i}{2} n_\perp n_\parallel \sum_j \frac{\omega_{pj}^2}{\omega \Omega_j} \frac{v_{thj}^2}{c^2} \sum_{n=-\infty}^{+\infty} \left[I_n(\lambda_j) - I_n'(\lambda_j)\right] e^{-\lambda_j} x_{0j}^2 Z'(x_{nj}) \\
\epsilon_{zz} &= 1 - \sum_j \frac{\omega_{pj}}{\omega^2} \sum_{n=-\infty}^{+\infty} I_n(\lambda_j) e^{-\lambda_j} \left(-x_{0j} Z(x_{nj})\right)
\end{aligned} \tag{1.2}$$

Here the coordinates are chosen so that z is parallel to the static magnetic field, and $\vec{k}$ lies in the (x, z)-plane. $k_\perp$ and $k_\parallel$ denote the perpendicular and parallel components of the wavevector, and $n_\perp = k_\perp c/\omega$, $n_\parallel = k_\parallel c/\omega$ those of the index. ω_{pj} and Ω_{cj} are the plasma and cyclotron frequencies, and $v_{thj}^2 = 2T_j/m_j$ the thermal velocity of species j. I_n is the modified Bessel function of order n, with argument

$$\lambda_j = k_\perp^2 v_{thj}^2 / 2\Omega_{cj}^2 \tag{1.3}$$

Finally, Z is the Plasma Dispersion Function [2], defined as

$$Z(\zeta) = \frac{1}{\sqrt{\pi}} \int_{-\infty}^{+\infty} \frac{e^{-u^2}}{u - \zeta} du + i\sigma\sqrt{\pi} e^{-\zeta^2} \tag{1.4}$$

with $\sigma = 0, 1, 2$ when $\mathrm{Im}(\zeta) > 0, = 0, < 0$, respectively, and

$$x_{nj} = \frac{\omega - n\Omega_{cj}}{k_{\|} v_{thj}} \tag{1.5}$$

The Dispersion Relation is the solubility condition for the algebraic form of Maxwell equations for a plane wave,

$$\underline{\underline{M}}_{\vec{k},\omega} \cdot \vec{E}_0 = \frac{c^2}{\omega^2} \vec{k} \times (\vec{k} \times \vec{E}_0) + \underline{\underline{\epsilon}} \cdot \vec{E}_0 = 0 \tag{1.6}$$

i.e.

$$H(\vec{k}, \omega) = \det | n^2 (\delta_{ij} - k_i k_j / k^2) - \epsilon_{ij}(\vec{k}, \omega) | = 0 \tag{1.7}$$

For applications to tokamaks it is appropriate as a first approximation to regard it as an equation for $k_{\perp}$, with ω and $k_{\|}$ real, fixed respectively by the generator and by the antenna periodicity. The discussion of this complicated equation is facilitated by a few general guidelines:

a) The order of magnitude of the compoments of $\underline{\underline{\epsilon}}$ are always the same as in the cold plasma limit, $v_{th} \to 0$, and cold plasma waves always play a fundamental role. In this limit, the only non vanishing components of the dilectric tensor (cfr. [1], Ch. 3) are:

$$\epsilon_{xx} = S = \frac{1}{2}(R + L) \qquad \epsilon_{xy} = -\epsilon_{yx} = -iD = -\frac{i}{2}(R - L) \qquad \epsilon_{zz} = P \tag{1.8}$$

with

$$R = 1 - \sum_j \frac{\omega_{pj}}{\omega^2} \frac{\omega}{\omega + \Omega_{cj}} \qquad L = 1 - \sum_j \frac{\omega_{pj}}{\omega^2} \frac{\omega}{\omega - \Omega_{cj}} \qquad P = 1 - \sum_j \frac{\omega_{pj}}{\omega^2} \tag{1.9}$$

The corresponding dispersion relation, written as a quadratic equation for $n_{\perp}^2$, is:

$$S n_{\perp}^4 - \left[RL + PS - n_{\|}^2 (P + S) \right] n_{\perp}^2 + P(n_{\|}^2 - R)(n_{\|}^2 - L) = 0 \tag{1.10}$$

b) The wavelength of most (although not all) waves is much greater than the average Larmor radius of all species. Hence finite temperature effects can be investigated by developing Eq. (1.7) to first order in $\lambda = k_{\perp}^2 \rho^2 / 2 << 1$. There is no small parameter allowing a similar expansion along the static magnetic field: in this direction the Z–functions have to be retained to describe dispersion and absorption correctly.

c) On the other hand, when $\vec{k} \to \infty$, i.e. when the phase velocity is much slower than the speed of light, the waves become essentially electrostatic, $\vec{E} \simeq -\vec{\nabla}\Phi = -i\vec{k}\Phi$. Then the dispersion relation can be well approximated by

$$\frac{k_i \epsilon_{ij}(\vec{k},\omega) k_j}{k^2} = 0 \tag{1.11}$$

It is also well–known that the power absorbed per unit volume is given by

$$P_{abs} = \frac{\omega}{8\pi} \vec{E}_0^* \cdot \underline{\underline{\epsilon}}^A \cdot \vec{E}_0 \tag{1.12}$$

where $\underline{\underline{\epsilon}}^A$ is the antihermitean part of the dielectric tensor. In particular, absorption is important when for $n = 0, \pm 1$ or $\pm 2 \cdots$ the condition

$$x_{nj} = \frac{\omega - n\Omega_{cj}}{k_\parallel v_{thj}} = O(1) \tag{1.13}$$

is satisfied. It should be also kept in mind, however, that the polarisation of each wave also plays an important role in determining the damping rate.

1.2 - Cold plasma waves at low frequencies. The ICR and LHR frequency ranges both lie well below the electron cyclotron frequency; since in tokamaks $\omega_{pe}/\Omega_{ce} = O(1)$, also well below the electron plasma frequency (this is true even at the plasma edge, although only by a small margin in the LH case):

$$\omega << \omega_{pe}, \Omega_{ce} \tag{1.14}$$

At these frequencies the electrons respond essentially in the drift approximation: $\vec{E} \times \vec{B}$ and polartisation drift in the perpendicular direction, free inertial motion in the parallel direction. Because of the smallness of the m_e/m_i ratio, P is always very large ($-P = O((m_i/m_e)^2)$ in the ICR range, $-P = O(m_i/m_e)$ in the LHR range). Using $|P|^{-1}$ as expansion parameter, the cold plasma dispersion relation can be accurately factorised as follows:

$$\text{Fast wave} \qquad n_{\perp,F}^2 = -\frac{(n_\parallel^2 - R)(n_\parallel^2 - L)}{(n_\parallel^2 - S)} \tag{1.15}$$

$$\text{Slow wave} \qquad n_{\perp,S}^2 = -(n_\parallel^2 - S)\frac{P}{S} \tag{1.16}$$

The Fast wave (FW) is known as Magnetosonic or Compressional Alfvén wave at low frequencies, and as Extraordinary wave at high frequencies; the Slow wave (SW) as

Shear Alfvén wave at low frequencies, and as Ordinary wave at high frequencies. The SW wave exhibits a perpendicular resonance ($k_\perp \to \infty$) when $S = 0$. This occurs in particular at the LH resonance. The denominations Fast and Slow refer to the relative values of the perpendicular phase velocities: the absolute value of root (1.15) is normally much smaller than that of (1.16) throughout the low frequency domain.

The above factorisation breaks down only when the condition $n_\parallel^2 = S$ is satisfied, so that the two roots must cross. In the LH frequency range this confluence influences the accessibility of the plasma core to externally launced slow waves. In the ICR domain, it must be regarded as a resonance of the fast wave. The meaning of the various cut–offs ($n_\perp^2 = 0$) will be discussed later.

1.3 - Finite Temperature effects. The development of the hot plasma dielectric tensor to first order in λ_j gives:

$$\begin{aligned} \epsilon_{xx} &= S - \sigma n_\perp^2 \qquad \epsilon_{yy} = S - \sigma' n_\perp^2 \qquad \epsilon_{zz} = P - \pi n_\perp^2 \\ \epsilon_{xy} &= -\epsilon_{yx} = -i(D - \delta n_\perp^2) \qquad \epsilon_{yz} = -\epsilon_{yx} = -n_\parallel n_\perp \xi \end{aligned} \tag{1.17}$$

Here

$$\begin{aligned} S &= \frac{1}{2}(R+L) \qquad\qquad D = \frac{1}{2}(R-L) \\ \sigma &= \frac{1}{2}(\rho+\lambda) + \tau \qquad \sigma' = \frac{1}{2}(\rho+\lambda) - \tau \qquad \delta = \frac{1}{2}(\rho-\lambda) \end{aligned} \tag{1.18}$$

with

$$\begin{aligned} R &= 1 - \sum_j \frac{\omega_{pj}}{\omega^2}(-x_{0j} Z(x_{-1j}) \qquad\qquad L = 1 - \sum_j \frac{\omega_{pj}}{\omega^2}(-x_{0j} Z(x_{+1j}) \\ P &= 1 - \sum_j \frac{\omega_{pj}}{\omega^2}(-x_{0e} Z(x_{0e}) \end{aligned} \tag{1.19}$$

and

$$\begin{aligned} \rho &= \frac{1}{2}\sum_j \frac{\omega_{pj}}{\omega^2}\frac{v_{thj}^2}{c^2}\left[-x_{0j}Z(x_{0j}) + 2x_{0j}Z(x_{-1j}) - x_{0j}Z(x_{-2j})\right] \\ \lambda &= \frac{1}{2}\sum_j \frac{\omega_{pj}}{\omega^2}\frac{v_{thj}^2}{c^2}\left[-x_{0j}Z(x_{0j}) + 2x_{0j}Z(x_{+1j}) - x_{0j}Z(x_{+2j})\right] \\ \tau &= \frac{1}{2}\sum_j \frac{\omega_{pj}}{\omega^2}\frac{v_{thj}^2}{c^2}\left[-x_{0j}Z(x_{0j}) + \frac{1}{2}\left(x_{0j}Z(x_{-1j}) + x_{0j}Z(x_{+1j})\right)\right] \\ \xi &= \frac{1}{4}\sum_j \frac{\omega_{pj}^2}{\omega\Omega_j}\frac{v_{thj}^2}{c^2}\left[x_{0j}^2 Z'(x_{0j}) - \left(x_{0j}^2 Z'(x_{-1j}) + x_{0j}^2 Z'(x_{+1j})\right)\right] \\ \pi &= \frac{1}{2}\sum_j \frac{\omega_{pj}}{\omega^2}\frac{v_{thj}^2}{c^2}\left[-x_{0j}^2 Z'(x_{0j}) + \frac{1}{2}\left(x_{0j}x_{-1j}Z'(x_{-1j}) + x_{0j}x_{+1j}Z'(x_{+1j})\right)\right] \end{aligned} \tag{1.20}$$

We recognise here two kinds of finite temperature effects. In the parallel direction, the complex Z–functions contribute an antihermitean part to the dielectruc tensor, which describe kinetic absorption when conditions (1.10) are satisfied. In the perpendicular direction, the FLR corrections take into account that in the plasma, in addition to waves driven by electromagnetic forces, also pressure–driven waves are possible, as in all fluids. Note that the FLR terms are proportional to β, the ratio of the plasma pressure to the 'pressure' of the static magnetic field.

Not all FLR corrections are equally important, however. From the fact that the $\vec{\nabla} \times (\vec{\nabla} \times \vec{E})$ operator is transverse (i.e. orthogonal to the wavevector), it easily follows that the most important one is the $-\sigma n_\perp^2$ correction to S. Indeed this term increases the order of the dispersion relation, making it into a cubic in $n_\perp^2$; it is thereby responsible for the existence of a new root, the expected pressure–driven wave. In the IC range however $|P|$ is so large that FLR corrections must be taken into account also in the coefficients of terms of lower order in $n_\perp^2$, when multiplied with P. An adequate approximation covering the whole low frequency range is

$$\begin{aligned} -\sigma n_\perp^6 + A n_\perp^4 - B n_\perp^2 + C &= 0 \\ A &= S + P\sigma \\ B &= -P\left[(n_\parallel^2 - S) + (n_\parallel^2 - L)\rho + (n_\parallel^2 - R)\lambda\right] \\ C &= P(n_\parallel^2 - R)(n_\parallel^2 - L) \end{aligned} \tag{1.21}$$

In addition to the two approximate cold plasma roots given by Eq. (1.14-15), this equation admits a new, hot–plasma root, which for most purposes can be simply approximated by

$$n_{\perp H}^2 \simeq \frac{S}{\sigma} \tag{1.22}$$

This wave bears different names in different frequency and plasma parameter domains. An appropriate name for this branch as a whole would be the acoustic wave; however, for historical reasons this name is reserved to a particular branch with $|x_{oe}| << 1$, which is heavily damped unless $T_i << T_e$, and therefore plays no role in Tokamak plasmas. For convenience, we will often refer to (1.22) as the pressure-driven wave. Because of its very large perpendicular index, this wave is always almost electrostatic.

FLR corrections will play a particularly important role in the vicinity of cold plasma resonances: as $S \to 0$, the slow cold–plasma root increases, and will finally cross the hot–plasma one. Thus the divergence of $k_\perp$ found in the cold plasma approximation is replaced by a confluence with the pressure–driven wave. A confluence of this kind

occurs near the LH resonance. In the ICR range, a confluence between the Fast wave and the hot–plasma branch also occurs near $\omega = 2\Omega_{ci}$, where σ is resonantly large, while S remains finite. In this case the wave (1.22) is known as the lowest Ion Bernstein wave (IBW). In a multi–species plasma, moreover, the condition $n_\parallel^2 - S = 0$ is satisfied near the Buchbaum ion–ion hybrid resonances [3]; this circumstance can also lead to a confluence between the FW and the IBW.

When in an inhomogeneous plasma an externally launched wave is incident upon a confluence, it is partly reflected, partly transmitted (if the optical thickness of the evanescence layer following the confluence is not too great), and partially mode converted into the slower branch of the dispersion relation. The latter is usually rapidly thermalised, since its phase velocity is low, and becomes comparable with the thermal velocity of particles at some distance from the conversion layer. Linear mode conversion is a fundamental ingredient of h.f. plasma heating.

It is perhaps not superfluous to recall that when developing the dispersion relation in powers of $k_\perp^2 \rho_i^2/2$, it is meaningful to retain only the first order corrections describing pressure–driven waves. If $k_\perp \rho_i$ is not small, taking into account higher order terms would introduce spurious roots, by approximating a transcendental equation with a polynomial one. The condition $k_\perp^2 \rho_i^2 << 1$ is actually violated by the slow wave and the pressure-driven wave near the LH resonance. In this case however the ion response to the wave is essentially unaffected by the static magnetic field; an expansion in the small parameter $k_\perp v_{thi}/\omega$ (thermal ion velocity over perpendicular wave phase velocity) leads again to Eq. (1.22) [4].

1.4 - Wave–particle interactions The rate of energy change of a particle in a plane wave, averaged over times much longer than ω^{-1}, is

$$\left\langle \frac{d}{dt} \frac{mv^2}{2} \right\rangle = Ze \left\langle \vec{v} \cdot \vec{E} \cos(\vec{k} \cdot \vec{x} - \omega t) \right\rangle \tag{1.23}$$

To the accuracy of the linear Vlasov equation the phase factor can be evaluated using the *averaged* motion only. In this approximation, the r.h. side of (1.23) is non-vanishing only for particles for which the Doppler shifted wave frequency is commensurable with some frequency of the periodic motion:

$$m(\omega - k_\parallel v_\parallel) = n\Omega_c \tag{1.24}$$

The most important cases are $m = 1$, with $n = 0$ (Landau and Transit Time) damping; $n = 1$ (Fundamental Cyclotron damping); and $n = 2$ (Harmonic Cyclotron damping).

Higher cyclotron harmonics are important only for wavelengths comparable or shorter than the Larmor radius. Harmonics of the wave frequency ($m > 1$) are negligible if the particle displacement is small compared to the wavelength, as it is almost always the case.

The dynamics of wave-particle interactions is however reversible. The secular "resonant" increase of kinetic energy describes only the initial phase of the motion: after a sufficiently long time trapping and bouncing occurs, with no average energy gain or loss. This is well illustrated by the example of electrons interacting with a one-dimensional electrostatic wave. The bouncing time of a trapped electron ($v_\parallel \simeq v_\phi = \omega/k_\parallel$) is in this case given by

$$\tau_B = \left(\frac{\pi}{2}\frac{m_e}{k_\parallel \Phi}\right)^{1/2} \tag{1.25}$$

In practice, reversibility is destroyed by collisions. A resonant electron is detrapped if its parallel velocity is changed by the small amount

$$\delta v_\parallel \simeq \left(-2\frac{e\Phi}{m_e}\right)^{1/2} \tag{1.26}$$

Since Coulomb collisions are a random–walk process, this requires a time

$$\tau_{det} \simeq \tau_{coll}(v_\phi)\frac{(\delta v_\parallel)^2}{v_\parallel^2} \simeq \nu_e^{-1}\frac{v_\phi^3}{v_{the}^3}\left(-\frac{e\Phi}{m_e v_\phi^2}\right) \tag{1.27}$$

Within τ_{det} a resonant particle is detrapped, and replaced by an equivalent one; if the collision rate changes slightly, the time during which a single particle remains in resonance changes, but this will be compensated by an opposite change of the replacement rate. Hence if τ_{det} is shorter than τ_B the damping rate will be independent from ν_e.

Under these conditions, collisions are able to mantain a Maxwellian distribution arbitrarily close to the resonant velocity. Hence, in particular, the condition

$$-\frac{e\Phi}{T_e} \lesssim \left(\frac{\nu_e}{\omega_{pe}}\right)^{2/3} \tag{1.28}$$

is also a sufficient condition for the validity of the linear Vlasov equation ("neoclassic" theory of heating, [5], [6]).

1.5 - Quasilinear description of heating At low frequencies antennas are necessarily of dimensions comparable or smaller than the wavelength. As a consequence, they cannot launch a single plane wave: instead, the radiated field will consist of a more or less broad superposition of such waves. In the presence of a spectrum of waves with closely spaced wavevectors,

$$\vec{E}(\vec{r},t) = \sum_j \vec{E}_j e^{i(\vec{k}_j \cdot \vec{r} - \omega t)} \tag{1.29}$$

the phase between a resonant particle and any one wave is perturbed by all other waves, whose phase velocities are also not far from resonance. Thus to the particle the wave phases appear random, even if they are not really so. Collisionless stochasticity of this kind can replace collisions to justify the linear description of plasma waves.

Under these conditions the long term evolution of the distribution function f_o is obtained by substituting into the nonlinear part of Vlasov equation the formal solution f_1 of the linearised equation, and by averaging the result over times $t >> \omega^{-1}$ ([7], [8]):

$$\left.\frac{\partial f_o}{\partial t}\right)_{QL} = -\frac{1}{2}\frac{Ze}{m}\left\langle \mathrm{Re}\left(\vec{E}^* \cdot \frac{\partial f_1}{\partial \vec{v}}\right)\right\rangle = \frac{\partial}{\partial \vec{v}}\left(\underline{\underline{D}}_{QL}(\vec{v})\frac{\partial f_o}{\partial \vec{v}}\right) \tag{1.30}$$

The general form of the quasilinear diffusion tensor in a uniform magnetized plasma has been derived in [9].

When the conditions for the quasilinear description are satisfied, the power absorbed per unit volume can be shown to be

$$\begin{aligned} P_{abs} = \sum_{spec} \frac{\omega}{8\pi}\frac{\omega_p}{\omega^2} \sum_j \int d\vec{v} f_o(\vec{v}) \\ 2\pi \sum_{n=-\infty}^{+\infty} \delta\left(\frac{\omega - n\Omega_c - k_{\parallel,j}}{\omega}\right) |\vec{V}_n \cdot \vec{E}(\vec{k}_j)|^2 \end{aligned} \tag{1.31}$$

where

$$\begin{aligned} \vec{V}_n \cdot \vec{E} = \frac{v_\perp}{\sqrt{2}}\left[J_{n-1}\left(\frac{k_\perp v_\perp}{\Omega_c}\right)E_+ + J_{n+1}\left(\frac{k_\perp v_\perp}{\Omega_c}\right)E_-\right] \\ + v_\parallel J_n\left(\frac{k_\perp v_\perp}{\Omega_c}\right)E_\parallel \end{aligned} \tag{1.32}$$

It is not difficult to see that this result could also be obtained by summing over the spectrum the expression (1.12) for a single plane wave.

2 - LOWER HYBRID HEATING.

2.1 - Lower Hybrid Resonance and Linear Turning Point. Lower Hybrid Heating relies on damping of the slow cold plasma wave, Eq. (1.16), at frequencies in the Ghz frequency range,

$$\Omega_{ci} << \omega << \Omega_{ce} \tag{2.1}$$

At these frequencies the ion respond as essentially unmagnetised. The elements of the cold plasma dielectric tensor then simplify to

$$S = 1 + \frac{\omega_{pe}^2}{\Omega_{ce}^2} - \sum_i \frac{\omega_{pi}}{\omega^2} \qquad D = -\frac{\omega_{pe}^2}{\omega\Omega_{ce}} \qquad P = -\frac{\omega_{pe}}{\omega^2} \tag{2.2}$$

The LH resonance is the frequency which makes $S = 0$:

$$\omega_{LH} = \sqrt{\frac{\omega_{pi}}{1 + \frac{\omega_{pe}^2}{\Omega_{ce}^2}}} \tag{2.2}$$

For a given frequency f (in Ghz), the resonance will occur at the density

$$n_{e,LH} = \frac{2.26\,10^{13} A_i f}{1 - 2.34 A_i f^2/B^2} \quad (\mathrm{cm}^{-3}) \tag{2.3}$$

Here f is the applied frequency in Ghz, and B_o the static magnetic field in Tesla. The resonance density increases with increasing frequency, and goes to infinity when $\omega \to \sqrt{\Omega_{ci}\Omega_{ce}}$; above this frequency there is no resonance.

In a hot plasma, the resonance is replaced by a confluence between the slow wave (1.16) and the hot plasma wave (1.22), known as Linear Turning Point, which occurs at a density slightly lower than the LH resonance. The FLR correction to ϵ_{xx} in this frequency range can be approximated as

$$\sigma n_\perp^2 = \frac{3}{2}\frac{\omega_{pi}^2}{\Omega_{ci}^2}\frac{v_{thi}^2}{c^2}\left(1 + \frac{1}{4}\frac{\omega^4}{\Omega_{ce}^2\Omega_{ci}^2}\frac{T_e}{T_i}\right) n_\perp^2 \tag{2.4}$$

(electron and ion contributions to σ are of the same order of magnitude). The position of the LTP can then be easily deduced from Eq. (1.21) by factorising away the fast root:

$$\frac{\omega_{pi}}{\omega^2} = \left[1 - \frac{\omega^2}{\Omega_{ce}\Omega_{ci}} + \frac{|n_\parallel|\sqrt{T - i}}{6.25}\sqrt{1 + \frac{1}{4}\frac{\omega^4}{\Omega_{ce}^2\Omega_{ci}^2}\frac{T_e}{T_i}}\right]^{-1} \tag{2.5}$$

An example of exact dispersion curves ($k_\perp$ versus density) in the vicinity of the LTP is shown in Fig. 1. One recognises a further conversion point to a third wave with

very short perpendicular wavelength, which moreover depends sensitively on the ratio ω/Ω_{ci}: it is a high–order Ion Bernstein wave, not described by the FLR dispersion relation (1.21), but only by the complete one (1.7). For the following discussion, it is useful to keep in mind that all these waves, because of the large value of $n_\perp$, are essentially electrostatically polarised (for the cold SW this holds as soon as $n_\parallel^2 \gtrsim S$; for the mode–converted waves always). The SW moreover is a backward wave, i.e. its perpendicular group velocity is opposite to the perpendicular phase velocity.

2.2 - Absorption mechanisms: a) ion heating. Hystorically, interest in the LH wave was motivated by its slow perpendicular phase velocity in the vicinity of the LH resonance. As the wave approaches resonance from the propagative side, both its phase and group velocity perpendicular to B_o tend to zero. Any dissipation mechanism, however weak, can then produce very strong damping. This is confirmed by solving the wave equation in the vicinity of the resonance layer. Taking advantage of the fact that in this region the wave must be essentially electrostatic, this equation can be simplified to

$$\frac{d}{dx}\left(S\frac{dE_z}{dx}\right) - \frac{c^2}{\omega^2}n_\parallel^2 P E_z = 0 \qquad (2.4)$$

(here x is the direction of the density gradient, assumed to be perpendicular to the static magnetic field). Approximating S by a linear function of x in the vicinity of the resonance $S = 0$, with a small imaginary part to take into account dissipation and guarantee causality, this equation becomes a particular case of Bessel equation. The solution satisfying the appropriate radiation conditions shows that there is no reflection (and of course no transmission, since the wave is evanescent on the high density side of the resonance): all power is absorbed. By placing the resonance so that $\omega/k_\perp$ becomes comparable to v_{thi} in the plasma core, it was hoped to heat the ions efficiently.

When finite temperature effects are taken into account, the wave equation becomes of fourth–order, the singularity of Eq. (2.4) being eliminated by the small higher order terms. With an elegant solution of this equation near the LTP using countour integration, Stix [10] has shown that an incident SW is completely mode–converted to the hot–plasma wave, again without reflection on the cold plasma branch. As the mode converted wave propagates back towards lower densities, its perpendicular phase velocity decreases, and becomes rapidly comparable to the ion thermal speed. Thus finally total absorption by the ions can again be expected.

Strictly speaking, the linear hot plasma dispersion relation predicts absorption by the ions to be localised in the vicinity of high–order cyclotron harmonics [4]: in the

antihermitean part of the dielectric tensor the effects of the magnetic field cannot be neglected, so that between harmonics the plasma remains transparent however slow the wave, as is clearly to be seen from fig. 1. A closer investigation shows however that this prediction is due to the fact that the linear theory attributes to the ions an infinite memory of the gyration phase, an assumption which is never realistic in practice.

Let us briefly comment on the ion absorption mechanism. During a cyclotron orbit, the phase of the electric field seen by an ion oscillates rapidly, since $\omega >> \Omega_{ci}$. If $\omega/k_\perp v_\perp > 1$, however, the phase is stationary twice per orbit (fig. 2). The resulting ion-wave interaction ressembles closely a Cerenkoff resonance, since the curvature of the ion orbit is clearly negligible to a first approximation. Then if a mechanism exists which decorrelates the phase between $\vec{E}_\perp$ and $\vec{v}_\perp$ rapidly enough, absorption of LH waves should become identic to Landau damping by non–magnetised ions. Such a mechanism is usually provided by the simultaneous presence of a spectrum of waves with slightly different phase velocities. Under these conditions, the long term evolution of the ion distribution function can be described in the quasilinear approximation. With the approximations suggested by the inequalities $\omega >> \Omega_{ci}$, $k_\perp v_{thi}/\Omega_{ci} \gtrsim 1$, Eq. (1.30) becomes ([13])

$$\frac{\partial f_i}{\partial t} = \frac{1}{v_\perp}\frac{\partial}{\partial v_\perp}\left[v_\perp D_{QL}(v_\perp)\frac{\partial f_i}{\partial v_\perp}\right] + \left(\frac{\partial f_i}{\partial t}\right)_{coll} \tag{2.5}$$

where the last term is the Fokker–Planck collision operator, and

$$D_{QL} = \frac{Z^2e^2}{2m_i^2\omega}\sum_{k_\parallel}\frac{(\frac{\omega}{k_\perp v_\perp})^3}{1+(\frac{\omega}{k_\perp v_\perp})^2}|E_x(k_\parallel)|^2 \qquad \left(\frac{\omega}{k_\perp v_\perp} > 1\right) \tag{2.6}$$

Ion absorption is then perpendicular Landau damping, which differs from Landau damping in the unmagnetized plasma only because the energy gained is immediately redistributed equally among the two perpendicular degrees of freedom by the gyration motion.

Even in the case of a narrow spectrum, moreover, the methods of modern Hamiltonian mechanics show that the ion motion becomes stochastic as soon as a very low threshold in the wave amplitude is exceeded, provided $k_\perp \rho_i \gtrsim 1$, where ρ_i is the Larmor radius ($\omega/k_\perp v_\perp \lesssim 1$ and $\omega >> \Omega_{ci}$ together imply that this condition is satisfied). Stochastic ion heating by LH waves has been studied in two very interesting papers by Karney [11], [12]. Karney has shown in particular that well above the stochasticity threshold equation (2.6) holds also in the monochromatic case.

A characteristic of perpendicular ion Landau damping is that the diffusion coefficient (2.6) is isotropic in the direction perpendicular to the static magnetic field, and is not localised in velocity space (Fig. 3): all ions whose perpendicular velocity is larger than the phase velocity are heated. Thus as soon as a few ions satisfy the resonance condition with the slowest waves in the spectrum, they will begin to gain perpendicular energy, and to interact also with faster waves, which would not be absorbed in a thermal plasma. Because of this synergetic effect, the predicted power deposition profile broadens considerably when the power is increased (Fig. 4, [13]). Above a few hundred kW in medium–size tokamaks, stochastic ion heating is expected to become very efficient as soon as:

$$\frac{\omega}{k_\perp v_{thi}} \gtrsim 6 \text{ to } 8 \tag{2.7}$$

and to produce tails of energetic ions with a large effective perpendicular temperature.

Experimentally however it has proved difficult, if not impossible, to achieve efficient ion heating with LH waves. At densities somewhat short of those which would be required for this purpose the waves cease to penetrate into the plasma core. The reason for this is not completely clear, although several mechanisms have been suggested, scattering by density fluctuations and/or depletion by parametric decay processes near the plasma edge being the most likely candidates. Fast ions are often seen e.g. by charge exchange diagnostics; hoverver in most cases they come from the plasma periphery, and appear to be accelerated by mechanisms different from the one sketched above.

2.3 - Absorption mechanisms: b) electron heating and current drive. Interest in the LH frequency range has nevertheless survived, and has even been dramatically fostered by the success of LH current drive. The possibility of sustaining the toroidal current necessary for the Tokamak equilibrium with LH waves was first discussed by Fisch [14]; the theory of CD was later developed in several papers by Fisch, Karney and others (for a review, see [15]). LHCD is based on Landau damping by electrons satisfying the parallel Cerenkoff resonance $\omega = k_\parallel v_\parallel$. The effects of this wave–particle interaction on the electron velocity distribution can again be described by a one–dimensional quasi–linear diffusion equation,

$$\frac{\partial f_e}{\partial t} = \frac{\partial}{\partial v_\parallel}\left[D_{QL}(v_\parallel)\frac{\partial f_e}{\partial v_\parallel}\right] + \left(\frac{\partial f_e}{\partial t}\right)_{coll} \tag{2.8}$$

where

$$D_{QL} = \frac{Z^2 e^2}{2m_i^2 \omega} \sum_{k_\parallel} \delta(\omega - k_\parallel v_\parallel)|E_z(k_\parallel)|^2 \tag{2.9}$$

In this case, quasilinear diffusion is localised to a well–defined range of parallel velocities, defined by the externally launched $k_{\|}$–spectrum. Since moreover under usual conditions the h.f. term is much larger than the collisional one (i.e. $D_{QL}/\nu_{coll}v_{the}^2 >> 1$), the electron distribution function develops a "plateau" in the corresponding velocity range (Fig. 5). An asymmetric spectrum, which can be realised by launching traveling waves, thus results in a net electron current. Collisions tend to reduce the plateau population by slowing down and scattering the electrons in pitch-angle; since collisionality decreases with energy, the efficiency of CD is expected to increase when the parallel phase velocity of the vawes increases, i.e. the parallel index decreases. This prediction is quantitatively confirmed experimentally.

It is unfortunately impossible to discuss in the space of these notes the very interesting and successful theory of LHCD; we must limit ourselves to a few comments on the points which are still not completely understood. The most puzzling is the so-called velocity gap paradox. It is intuitively clear that the 'heigth' of the plateau should be roughly proportional to the number of electrons near the slowest waves in the spectrum (cfr. Fig. 5). Indeed, while the efficiency, i.e. the ratio J/P (current to power required) is expected to increase when faster waves are used, J and P separately should decrease exponentially (as $exp\left\{-(\omega/k_{\|}v_{the})^2_{min}\right\}$). It was a fortunate circumstance that in the first investigations of LHCD emphasis was put on the efficiency J/P, rather that on J and P separately: otherwise LHCD might at first have encountered considerably less enthusiasm among experimentalists!

In the experiments however all the power having access to the plasma core is absorbed, so that not only the efficiency, but the current itself is optimised when the wave spectrum is optimised according to Fisch theory. To explain this behaviour, it is necessary to postulate a mechanism capable of extracting electrons from the bulk thermal population and to feed the quasilinear plateau across the velocity gap in the spectrum. This mechanism must require relatively little power, so as not to deplete the spectrum of waves launched from outside: any explanation invoking a substantial difference between the externally excited spectrum and the spectrum driving the current would be in sharp contrast with the experimental evidence [16], [17]. Moreover, bridging of the velocity gap seems to occur in the plasma center more or less independently of the width of the velocity gap there, yet never at the plasma periphery. Such a mechanism has not yet been unequivocally identified.

I would like to stress here that the velocity gap is a problem for the theoreticians, not for the plasma, who is perfectly happy with waves as fast as compatible with the

accessibility limit to be mentioned below. In the literature one reads from time to time suggestions to 'help' LHCD by in some way increasing the electron population in the velocity gap. Such methods might be useful only if they extend the density range in which the plasma is capable of sustaining a large population of suprathermal (but non run–away) electrons. As long as this is the case, LH waves approach the maximum theoretical efficiency with no external help, even if we do not really understand how.

The last remark naturally introduces the second problem of LHCD, namely the existence of a density limit above which the efficiency rapidly drops to essentially zero. The critical density for LHCD is within a factor 2 of the penetration limit mentioned above, although the two effects are probably distinct. Both limits scale empirically as the square of the applied frequency, a fact that has favored the use of higher frequencies. There are however technical limitations, which come in particular from constraints on the miniaturisation of the launching structure.

2.4 - Coupling and accessibility. After this rather superficial overview of the heating and current drive mechanisms, we turn to propagation and launching of LH waves. Fig. 6 shows the qualitative behaviour of $n_\perp^2$ with varying density (or with the distance from the plasma edge), for different values of the parallel index. A very important feature of these dispersion curves is the presence of a cut–off, $n_\perp^2 = 0$, at low density. For the slow wave the cut-off is at the density where $P = 0$, i.e.

$$n_e \quad (\mathrm{cm}^{-3}) = 1.24\ 10^{10} f^2 \tag{2.10}$$

while the cut–off of the fast wave is at

$$n_e \quad (\mathrm{cm}^{-3}) = 3.47\ 10^{11} |n_\parallel^2 - 1| B_o f \tag{2.11}$$

This means that a wave propagating inside the plasma is necessarily evanescent in vacuum: $n_\parallel^2 > 1$, $n_\perp^2 = 1 - n_\parallel^2 < 0$. Such waves can be excited only with a slow–wave structure. The cut–off density of the slow wave is so low that waves excited by such a structure will easily tunnel through the evanescence region, provided the antenna is placed close enough to the plasma surface. The cut–off density of the fast wave, on the other hand, is appreciably higher: coupling of the fast wave will accordingly be much less efficient under otherwise similar conditions.

From Fig. 6 it can furthermore be seen that waves with low $n_\parallel$ encounter a confluence with the fast wave followed by a layer of evanescence between the plasma edge and the

LTP. Waves which do not satisfy this condition are trapped between the wall and the confluence, and excluded from the plasma interior. To avoid this confluence, a somewhat more stringent condition than evanescence in vacuum ($n_\parallel^2 > 1$) has to be satisfied in practice, namely [20]:

$$|n_\parallel| \geq \sqrt{1 + \frac{\omega_{pe}^2}{\Omega_{ce}^2} - \sum_i \frac{\omega_{pi}}{\omega^2}} + \sqrt{\frac{\omega_{pe}^2}{\Omega_{ce}^2}} \tag{2.12}$$

This accessibility condition is not in itself in contraddiction with Cerenkoff absorption by the electrons, nor does it impose further severe constraints on the antenna design. At high densities however, it can limit the efficiency of Current Drive by setting an upper limit on the parallel phase velocity of the waves which can reach the plasma core.

The nature of the required launching structure can be further clarified by exhamining the limit polarisation of each wave at vanishing density. In vacuum, the slow wave requires a toroidally oriented electric field (E_z), the fast wave a poloidally oriented one (E_y). This is again a distinctive advantage for the slow wave, which can be launched by a phased array of waveguides mounted flush on the plasma vessel with their short edge in the toroidal direction. This arrangement, originally suggested by P. Lallia [18] and known as Grill, allows great flexibility in the shaping of the launched spectrum, and would be easy to incorporate in the design of a reactor. The Grill has been successfully used in many heating and current drive experiments, and its coupling properties are well understood [19].

Waveguide coupling of the fast wave, on the other hand, although not impossible, would be much more difficult. The guides must be aligned with their longest side in the toroidal direction: this not only requires a lot of space between magnetic field coils, but is incompatible with the requirement $n_\parallel^2 > 1$ unless ridged or dielectrically loaded guides are used.

The description of Grill coupling is greatly simplified by neglecting the finite heigth of the guides in the poloidal direction. Then the field in each guide is a superposition of the fundamental TEM mode, and of evanescent TM modes excited at discontinuity represented by the openings of the guides on the plasma chamber:

$$\begin{aligned} E_z^g &= E_o \sum_{p=1}^{N} \Theta_p(z) \sum_{n+0}^{\infty} \left\{ \alpha_{np} e^{i\gamma_n x} + \beta_{np} e^{-i\gamma_n x} \right\} \cos \frac{n\pi(z - z_p)}{b} \\ B_y^g &= -E_o \sum_{p=1}^{N} \Theta_p(z) \sum_{n+0}^{\infty} \frac{1}{\gamma_n} \left\{ \alpha_{np} e^{i\gamma_n x} - \beta_{np} e^{-i\gamma_n x} \right\} \cos \frac{n\pi(z - z_p)}{b} \end{aligned} \tag{2.13}$$

where $\Theta_p(z)$ is unity in front of the p–th guide, $z_p \leq z \leq z_p + b$, and zero elsewhere, and

$$\begin{aligned} \gamma_o &= \frac{\omega}{c} && \text{propagating mode} \\ \gamma_n &= i\frac{\omega}{c}\left(\frac{n^2\pi^2}{b^2} - 1\right)^{1/2} && \text{evanescent modes } (\alpha_{np} \equiv 0) \end{aligned} \tag{2.14}$$

The excitation configuration is described by the complex coefficients α_{op}, which can be chosen arbitrarily; the reflection coefficients β_{op} and the coefficients β_{np} of the evanecent modes must be evaluated. In the plasma, the field is written as usual as a superposition of plane waves of the form

$$E_z^p = \int_{-\infty}^{+\infty} E_z^p(k_\parallel, x) e^{ik_\parallel z} \qquad B_y^p = \int_{-\infty}^{+\infty} B_y^p(k_\parallel, x) e^{ik_\parallel z} \tag{2.15}$$

where $E_z^p(k_\parallel, x)$, $B_y^p(k_\parallel, x)$ are the solution of the wave equations in the plasma which satisfies outgoing radiation conditions. The ratio

$$\frac{B_y^p(k_\parallel, 0)}{E_z^p(k_\parallel, 0)} = Y(k_\parallel) \tag{2.16}$$

for such waves is the surface admittance of the plasma for plane waves. Assuming a linear density profile near the plasma edge, $Y(k_\parallel)$ can be expressed in terms of Airy functions; for most purpose, an adequate approximation is

$$Y(n_\parallel) \simeq \frac{1}{|n_\parallel^2 - 1|^{1/6}} \tag{2.17}$$

In the plane of the guide mouths, $x = 0$, E_z must be continuous everywhere (in particular, it must vanish on the metallic wall). This implies the identity of the z–Fourier transform of $E_z^g(x = 0)$ with $E_z^p(k_\parallel, 0)$. The Fourier spectrum of $B_y(x = 0)$ on the plasma side, $B_z^p(k_\parallel, 0)$, must be related to $E_z^p(k_\parallel, 0)$ by Eq. (2.16). In the plane $x = 0$, however, B_y is continuous only at the guide apertures (in the wall currents will generally flow). Exploiting the orthogonality of the waveguides eigenmodes, this condition can be transformed into a set of linear equations for the unknown coefficients β_{np}, which is solved numerically. This allows to evaluate the reflection (in amplitude and phase) in each guide. The total reflection R is a function of the phase $\Delta\Phi$ between guides (Fig. 7), and, for a given $\Delta\Phi$, of n_e and dn_e/dx at the plasma edge; for $\Delta\Phi = 90^o$ or 180^o, R has a shallow minimum of the order of a few percent or less (Fig. 8). The agreement with coupling measurement is usually quite good, to the point that the

reflection coefficients measured in the different guides are considered a reliable indication of the plasma density in front of the Grill.

The most important output of the Grill theory is however the radiated power spectrum:

$$P_x(n_\parallel) = Cte \cdot |E_z^p(k_\parallel, 0)|^2 \cdot \frac{\mathrm{Re}\,(Y(n_\parallel))}{|n_\parallel^2 - 1|^{1/2}} \qquad \left(n_\parallel^2 > 1\right) \tag{2.18}$$

The functional dependence of the r.h. side on $k_\parallel$ favours somewhat waves with low parallel index. Thus it is difficult to satisfactorily shape the spectrum with only two waveguides: the spectrum of a two–guide Grill is always "triangular". Grills with 4 guides or more however allow great flexibility: the $k_\parallel$–depence of the surface admittance is relatively slow, and the spectrum is dominated by the form factor $|E_z|^2$, which can be directly manipulated by phasing the guides, as long as reflection is low. An example of power spectra from a Grill with 8 waveguides excited with equal amplitudes and different phases is shown in Fig. 9.

One should however be aware that the freedom of spectral shaping is limited by the properties of Fourier transforms. Thus the finite length of the antenna, and the fact that evanescent guide modes excited at the guide mouths radiate somewhat at larger values of $n_\parallel$, put an upper limit of about 0.8 to the directivity which can be achieved in view of Current Drive.

2.5 - Resonance cones. Let us briefly mention another peculiar property of LH waves. In the electrostatic approximation, the direction of their group velocity does not depend on the value of $k_\parallel$:

$$\frac{v_{g\perp}}{v_{g\parallel}} = \frac{\partial H/\partial z}{\partial H/\partial x} = \pm \left(\frac{m_e}{m_i}\right)^{1/2} \left(\frac{\omega^2 - \omega_{LH}^2}{\omega_{LH}^2}\right)^{1/2} \tag{2.19}$$

This has the consequence that the field excited by a finite length antenna is localised along the bundles of "rays"

$$dx/dz = v_{gx}/v_{gz} \tag{2.20}$$

from the antenna itself (known as resonance cones). Resonance cones where discovered by Kuehl [21]; their effect on LH waves launching was studied by Bellan and Porkolab [22]. Note that at the frequencies of interest in tokamaks, LH resonance cones make an angle of order $(m_e/m_i)^{1/2}$ with the static magnetic field: this implies that LH waves have to travel a very long optical length to reach the plasma core.

To get more feeling for resonance cones, it is useful to start from the cold Poisson equation

$$\frac{\partial}{\partial x}\left(\epsilon_{xx}\frac{\partial \Phi}{\partial x}\right)+\frac{\partial}{\partial z}\left(\epsilon_{zz}\frac{\partial \Phi}{\partial x}\right)=0 \tag{2.21}$$

(Eq. (2.4) is a particular case of this equation). In the LH domain, Poisson's equation is hyperbolic and admits wave–like solutions because $\epsilon_{xx}/\epsilon_{zz} = S/P < 0$; the "rays", solutions of the ray equations (2.20), are its characteristic, and can be used to construct the solution which satisfies given boundary conditions. Assuming the applicability of the WKB approximation (i.e. that S and P vary slowly on the scale of the SW wavelength), the general solution can be written:

$$\Phi(x,z)=\Phi_+(z-g(x,z))+\Phi_-(z+g(x,z)) \tag{2.22}$$

where $z=\pm g(x,z)$ are the equation of the two rays through the point z from appropriate points in the antenna plane $x=0$. The functions $\Phi_\pm$ are arbitrary, except for the condition that no power must come from infinity toward this plane. By considering the Fourier decomposition of the antenna field in the z–direction, it is not difficult to show that to satisfy causality the signal going to the right (Φ_+) must contain only partial waves with positive $k_\parallel$, the signal going to the left only waves with negative $k_\parallel$. This has an obvious interpretation in terms of group velocity; but it complicates somewhat the explicit imposition of given boundary conditions. Nevertheless, in simple cases the single–sided Fourier integrals can be evaluated, and the field pattern can be written in closed form.

This is the case for the electric field launched by a Grill of N guides phased by $\Delta\phi$, which in the $x=0$ plane can be fairly well simulated by the boundary condition

$$E_z(x=0,z)=E_o\sum_{p=1}^{N}\Theta_p(z)e^{ip\Delta\phi} \tag{2.23}$$

In this case one finds

$$E_z^{\pm}(x,z)=E_o\frac{S(0)P(x)}{S(x)P(0)}^{1/2}\sum_{p=1}^{N}e^{ip\Delta\phi}\left\{\frac{\Theta_p(z\mp g(x,z))}{2}+\frac{i}{2\pi}\log\left|\frac{z-(z_p\mp g(x,z))}{z-(z_p+b\mp g(x,z))}\right|\right\} \tag{2.24}$$

This shows that the field in each Resonance Cone is not just the image of the field of the antenna enhanced by the usual WKB factor, as it is often assumed. A logarithmic singularity develops along the rays which start from each discontinuity at the boundary (here the edges of each waveguide). Moreover the field from an antenna of finite length

decreases relatively slowly in the parallel direction away from the Resonance Cones, namely as

$$\Phi_{\pm} = O\left(\frac{1}{|z \pm g(x,z)|}\right) \qquad \text{for} \quad |z \pm g(x,z)| \to \infty \tag{2.25}$$

Note that both the singularity and the slowly decreasing tail in the field pattern are in quadrature with the field at the antenna, and do not contribute to the transport of power.

Of course, the singularity is a consequence of the approximations made: thus it can be removed by taking into account the decrease of tunneling efficiency from the antenna for waves with large $n_{\|}$ predicted by the Grill analysis. Nevertheless, at least in the plasma periphery, strong localised peaks of the electric field intensity must be expected. They are likely to be responsible for the sensitivity of LH waves to parasitic nonlinear effects near the plasma edge (parametric decay, filamentation, etc), and might thus indirectly play a role in the penetration problems encountered at high density.

Further inside the plasma, Resonance Cones need not be taken as seriously. Two effects severely limit the radial range over which their coherence can be maintained, even disregarding non–linear phenomena. First, electromagnetic corrections to the dispersion relation, although small, are cumulative. They make waves with smaller $n_{\|}$ penetrate radially slower than predicted by the electrostatic approximation, and thus broaden the illuminated region along B_o. This effect will be particulary strong for the 'fast' wavepackets which optimise CD efficiency: as $n_{\|}$ approaches the accessibility condition, field localisation is completely lost, since the fast wave does not form Resonance Cones. Secondly, the $n_{\|}$–spectrum reaching the plasma core is limited from above by electron Landau damping. Obviously, the field pattern cannot possess features with a spatial scale along B_o finer than the minimum parallel wavelength not yet absorbed.

2.6 - Toroidal effects. Throughout the preceding discussion, it has been tacitly assumed that $k_{\|}$ is constant during the propagation of LH waves. In a tokamak, this is only approximately true; instead, because of axisymmetry, the field can be Fourier analysed in ϕ (toroidal angle), and the constant component of the wavevector is the toroidal wavenumber n_{ϕ}. When the poloidal static magnetic field is taken into account,

$$k_{\|} \simeq \frac{n_{\phi}}{R} + \frac{B_{\theta}}{B_{\phi}} k_{\theta} \tag{2.26}$$

k_{θ} is essentially zero at the antenna, but needs not to remain zero in the plasma because of refraction.

The effects of toroidal geometry on the propagation of LH waves can be investigated by taking advantage of their short wavelength. This justifies the Eikonal Ansatz [23]–[24] (for a review, cfr. [25]):

$$\vec{E}(\vec{r},t) = \vec{E}_o(\vec{r},t)e^{i(S(\vec{r},t)-\omega t)} \tag{2.27}$$

The phase $S(\vec{r},t)$ is supposed to vary on a scale much faster than the amplitude and the equilibrium quantities, and defines the local wavenumber through

$$\vec{k} = \vec{\nabla} S \tag{2.28}$$

When (2.27) is substituted into Maxwell equations, to lowest order in the geometric optic expansion one finds that $\vec{k}$ must satisfy the Dispersion Relation $H(\vec{k},\omega) = 0$, which is thereby interpreted as a non–linear first–order partial differential equation for $S(\vec{r},t)$; its characteristics are the rays of geometric optics. The integration of the corresponding system of ordinary differential equations (Ray Tracing)

$$\frac{\partial \vec{r}}{\partial S} = D^{-1}\frac{\partial H}{\partial \vec{k}} \qquad \frac{\partial \vec{k}}{\partial S} = -D^{-1}\frac{\partial H}{\partial \vec{r}} \qquad \text{with} \quad D = \vec{k}\cdot\frac{\partial H}{\partial \vec{k}} \tag{2.29}$$

provides direct insight into the field pattern. From the next order in the expansion one obtains an equation for the propagation of power along the rays.

One should not overlook the fact, however, that the field radiated by a slow wave structure is necessarily dominated by diffraction. The way out of this difficulty is to exploit axisymmetry to Fourier–decompose the total field in the toroidal direction, and to apply Ray Tracing separately to each partial wave. In addition, the power transport equation can then be integrated along each ray, with initial conditions given by the theory of the antenna; in this way power deposition profiles can be easily evaluated.

The example shown in Fig. 10-11 illustrates the tendency of refraction to reduce the value of $k_\parallel$ with respect to the initial value at the antenna: this effect is negligible at low densities ($\omega^2/\omega_{pe}^2 \lesssim 0.1$), but increases the severity of the accessibility condition at intermediate and high densities. In Fig. 10 the central ray is followed for different initial values of $n_\parallel$: for large $n_\parallel$ all rays tend to follow the same path, as predicted by the electrostatic approximation, while waves with lower values of $n_\parallel$ penetrate more slowly. This makes visible in toroidal geometry the behaviour already discussed in the slab approximation. Because of the toroidal downshift in $n_\parallel$, a relatively broad portion of the spectrum penetrates almost to the plasma center without appreciable absorption, and is reflected before reaching the magnetic axis by "whispering gallery" phenomenon [24]. When the outgoing wave is reflected once again from the plasma surface and

propagates again inward, there is then a finite probability that its $n_\parallel$ undergoes a rapid upshift. With a quantitative investigation Bonoli [26] has suggested that this effect could fill the gap in phase velocities, and explain the already discussed Current Drive paradox.

2.7 - Conclusions. LH waves have very attractive features as far as generation and coupling is concerned, and have proved to be the best candidate for h.f. current drive. They are however truly "collective" plasma waves, i.e. their properties are quite different from those of h.f. waves in vacuum or in ordinary dielectrics. As a consequence of the strong electric fields along resonance cones, and of the long path they must travel to reach the plasma core, they are very sensitive to changes in the plasma parameters, and to depletion by parasitic effects which are not easy to identify and understand theoretically. While at low densities these effects seem to contribute to the success of Current Drive by broadening the $k_\parallel$–spectrum, at higher densities they make penetration problematic. This must be taken into account when evaluating the reactor prospects of LH waves.

3 - ION CYCLOTRON RESONANCE HEATING.

3.1 - Heating mechanism. In its simplest form, Ion Cyclotron Resonance Heating exploits the secular acceleration of ions by the left-hand circular component of $\vec{E}$ when the resonance condition

$$\omega - k_\parallel v_\parallel = \Omega_{ci} \tag{3.1}$$

is satisfied. An appreciable number of ions will simultaneously satisfy this condition if

$$\frac{\omega - \Omega_{ci}}{k_\parallel v_{thi}} = O(1) \tag{3.2}$$

Taking into account the horizontal variation of the magnetic field strength in a tokamak, this defines a vertical layer around the cyclotron resonance $\omega = \Omega_{ci}$, of width

$$(\Delta X)_{Res} \simeq 2n_\parallel \frac{v_{thi}}{c} R_o \tag{3.3}$$

The phase ξ between E_+ and the gyration velocity of an ion moving along a magnetic field line is stationary at the point where condition (3.1) is satisfied. If the parallel velocity is sufficiently large so that the parallel acceleration $\vec{\mu} \cdot \vec{\nabla} B$ can be neglected, it is not difficult to show that the resonance duration (the time during which $|\xi| \lesssim \pi/2$) is

$$\tau_R \simeq \left(\frac{\pi R^2 q}{\Omega_{ci} r |v_\parallel \sin\theta|} \right)^{1/2} \tag{3.4}$$

(The horizontal projection of the path of a single ion during the resonance time, $\Delta R \simeq \left(\pi r |v_\parallel \sin\theta| / \Omega_{ci} q\right)^{1/2}$, should not be confused with the region of strongest damping defined by Eq. (3.2)). During this time the perpendicular velocity of the ion changes from $v_\perp$ to

$$\left| v_\perp + \frac{ZeE_+}{m_i} e^{i\xi_o} \left(\frac{2\pi R^2 q}{r\Omega_{ci} |v_\parallel \sin\theta|} \right)^{1/2} \right| \tag{3.5}$$

Here r, θ are polar coordinates in the poloidal cross-section, R is the distance from the vertical axis, and $q = rB_\phi / RB_\theta$ the safety factor; ξ_o is the phase at some reference point along the ion trajectory. Averaging over ξ_o and taking into account that there are two resonances per connection length $2\pi qR$, one obtains an estimate of the rate of increase of the ion perpendicular energy $K_\perp$, namely

$$\frac{dK_\perp}{dt} \simeq \frac{Z^2 e^2 R}{m_i \Omega_{ci} r |\sin\theta|} |E_+|^2 \tag{3.6}$$

(for obvious geometrical reasons this estimate does not hold on the magnetic axis and when the magnetic surface is just tangent to the resonance; this however concerns a very small number of particles).

Under usual conditions, the fractional energy change of an ion at each crossing of the resonance is small; moreover it is reasonable to expect phase correlations between the waves and the ion to be destroyed (by collision and/or by the simultaneous presence of a broad spectrum of waves with different $k_\parallel$) in a time much shorter than the time of flight between two passages through resonance. Under these conditions, heating can be described as a hf–driven diffusion in velocity space. The long–term evolution of the ion distribution function obeys an equation of the quasilinear type [27]:

$$\frac{df_i}{dt} = \frac{1}{v_\perp} \frac{\partial}{\partial v_\perp} \left(v_\perp D_{QL} \frac{\partial f_i}{\partial v_\perp} \right) + \left(\frac{\partial fi}{\partial t} \right)_{coll} \tag{3.7}$$

where

$$D_{QL} = \left\langle \frac{\Delta v_\perp^2}{\Delta t} \right\rangle_{\xi_o} \simeq \frac{1}{m_i} \frac{dK_\perp}{dt} \tag{3.8}$$

and the last term is the Fokker-Planck collision operator.

The fundamental cyclotron resonance however cannot be made into a working ICRH method for tokamak plasmas without some refinement. As we will see in the next section, the natural way to perform ICRH in axisymmetric toroidal geometry is by launching the Fast Wave, Eq. (1.15), which in this frequency range is also known as the compressional Alfvén wave. This name comes from ideal MHD, which is a valid

description of HF waves in the limit $\omega/\Omega_{ci} \rightarrow 0$. Its use here is however perfectly justified, since the properties of the fast wave are little influenced by finite ω/Ω_{ci} effects. In particular, its perpendicular index (1.15) remains finite and well behaved at the cyclotron resonance itself: L and S diverge together, so that

$$\lim_{\omega \rightarrow \Omega_{ci}} (n_\perp^2)_F = -2(n_\parallel^2 - R) \tag{3.9}$$

How this is possible can be understood by inspection of the wave polarisation, which with good accuracy is given by

$$\frac{E_+}{E_-} = \frac{n_\parallel^2 - R}{n_\parallel^2 - L} \tag{3.10}$$

It follows that for $k_\parallel = 0$ the left–handed component E_+ vanishes at the cyclotron resonance, $L \rightarrow \infty$, so that the resonant ion current $(4\pi/\omega)J_+ = LE_+$ remains finite. In other words, the resonant response of the ions completely screens the component of the field which would be absorbed.

In practice, $k_\parallel$ is not zero: a finite length antenna always excites a relatively broad $k_\parallel$ spectrum (cfr. below), even if centered at $k_\parallel = 0$. For finite $k_\parallel$, L does not actually diverge at $\omega = \Omega_{ci}$, but in the resonance region is nevertheless very large, $L \simeq (\omega_{pi}^2/\Omega_{ci}^2)(\omega/k_\parallel v_{thi}) >> 1$. The fractional absorption through the resonance layer (3.8) can then be estimated by integrating the power balance equation

$$\frac{dP_x}{dx} = -\frac{\omega}{8\pi}\mathrm{Im}(L)|E_+|^2 \tag{3.11}$$

across this layer, with $\mathrm{Im}(L) = \sqrt{\pi}(\omega_{pi}^2/\Omega_{ci}^2)x_o e^{-x_1^2}$. Taking into account that the incident flux is

$$P_x = \frac{c}{8\pi} n_\perp |E_y|^2 \tag{3.12}$$

and using the above estimates for the polarisation, it is not difficult to obtain:

$$\frac{\Delta P_x}{P_x} \simeq \left(\frac{\omega}{c}R\right)\left(\frac{\omega_{pi}^2}{\Omega_{ci}^2}\right)^{1/2} n_\parallel^2 \frac{v_{thi}^2}{c^2} \tag{3.13}$$

Because of the very small factor $n_\parallel^2 v_{thi}^2/c^2$, the efficiency of fundamental ICRH in a single species plasma using the fast wave is expected to be uninterestingly low.

The simplest way to overcome this difficulty is to heat at a frequency equal twice the cyclotron frequency (we will call this frequency the first harmonic; in the american literature, however, it is often called second harmonic). First harmonic heating is a

finite Larmor radius effect. Indeed, when $\omega = 2\Omega_{ci}$, the sign of $\vec{E}_\perp \cdot v_\perp$ changes twice per cyclotron orbit; in a spatially homogeneous electric field the energy gained during half of the gyration period would be lost during the other half, with no net effect. If the wave has a finite perpendicular wavelength, however, the field seen in the two halves of the Larmor orbit is different, and cancellation is incomplete. From the equations of motion one easily obtains for the heating rate of a single particle

$$\frac{dK_\perp}{dt} \simeq \frac{Z^2 e^2 R}{m_i \Omega_{ci} r |\sin\theta|} |E_+|^2 n_\perp^2 \frac{v_\perp^2}{c^2} \tag{3.14}$$

while the fractional absorption through the resonance layer can be estimated to be

$$\frac{\Delta P_x}{P_x} \simeq \left(\frac{\omega}{c} R\right) \left(\frac{\omega_{pi}^2}{\Omega_{ci}^2}\right)^{1/2} n_\perp^2 \frac{v_{thi}^2}{c^2} \tag{3.15}$$

Thus the efficiency of first harmonic heating will be about $k_\perp^2/k_\parallel^2$ times larger than that of fundamental heating. From the FW dispersion relation $k_\perp^2/k_\parallel^2 \simeq \omega_{pi}^2/\Omega_{ci}^2 \simeq 30$ to 50; this factor is large enough to make first harmonic ICRH attractive. A favorable feature is moreover the fact that the efficiency is predicted to increase with increasing ion density and temperature.

When first harmonic ICRH heating was first attempted in small and relatively cool deuterium plasmas, the observed heating rate was even considerably higher than expected theoretically [28]. This was soon attributed [29] to the presence of a small fraction of H^+ ions, whose fundamental resonance coincides with the first harmonic of the majority D^+ species. At low concentration, the H^+ ions cannot screen the E_+ component efficiently, so that the wave polarisation is determined by the majority. Then the minority species can then be heated with very high efficiency. Minority heating has since become the most popular ICRH scheme. The coincidence between the minority fundamental and the majority first harmonic is not a necessity: thus minority heating of He_3^{++} in H^+ or D^+ has been successfully attempted, and can be even more efficient than H^+ in Deuterium [30].

ICRH tends to produce suprathermal ions with large perpendicular energy. This can be qualitatively understood by observing that according to Eqs. (3.6) and (3.14), the quasilinear diffusion coefficient (3.7) does not decrease (in the case of first harmonic heating it even increases) at large velocities. In the minority case moreover the power available per minority ion can be very large, so that they can reach quite high energies before thermalising it on the majority and on the electrons. Approximate expressions for the ion distribution functions under these conditions have been obtained by Stix

[31] by solving Eq. (3.7); they appear to be in excellent agreement with experimental charge exchange measurements. In some ICRH scenarios the presence of non negligible populations of suprathermal ions can be exploited to enhance the yeld of thermonuclear reactions.

Before turning to propagation and coupling, let us make a last comment about electron heating in the IC frequency range. The $k_\parallel$ spectrum of usual antennas is broad enough so that the Cerenkov condition $\omega/k_\parallel v_{the} \lesssim 1$ is easily satisfied in the plasma core. Nevertheless electron Landau damping is always negligible, since E_z is far too small:

$$\frac{E_z}{E_x} = \frac{n_\parallel n_\perp}{n_\perp^2 - P} = O\left(\frac{m_e}{m_i}\right)^{3/2} \tag{3.16}$$

(in this frequency range, electron Landau damping is negligible also for Bernstein waves, cfr. section 3.4). The Fast wave however can be damped by electron Transit Time, which is similar to Landau damping, except for the fact that it is driven by the $\vec{\mu} \cdot \vec{\nabla} B$ force, rather than by E_z. In Eq. (1.9) electron Transit Time is decribed by the FLR contribution of the electrons to ϵ^A_{yy}:

$$\left.\frac{dP_x}{dx}\right|_e = -\frac{\omega}{8\pi}\delta\left(\epsilon^A_{yy}\right)_e |E_y|^2 = \frac{\omega}{8\pi}\frac{\omega_{pe}^2}{\Omega_{ce}^2}\frac{v_{the}^2}{c^2}\sqrt{\pi}\frac{\omega}{k_\parallel v_{the}} e^{-\left(\frac{\omega}{k_\parallel v_{the}}\right)^2} |B_z|^2 \tag{3.17}$$

Being a finite Larmor radius effect, its efficiency increases with β: in a medium–size tokamak it is negligible as long as T_e is lower than 3 to 5 keV, but in a reactor plasma it could account for a sizable fraction of the total absorbed power ($\lesssim$ 50 %), at the expenses of ion heating.

3.2 - Ion–ion Resonances and Cut–offs. Eq. (1.15) is the exact form of the cold plasma dispersion relation in the limit of zero electron inertia ($-P = O((m_i/m_e)^2) \to 0$). In a single species plasma, L and S are both positive if $\omega < \Omega_{ci}$ and negative if $\omega > \Omega_{ci}$, and change sign only at the common singularity $\omega = \Omega_{ci}$, so that $n_\perp^2)_F$ remains regular. This is possible because, as already mentioned, $E_+ \to 0$ so that J_+ remains finite. The oscillating magnetic field is parallel to the static one, whence the name of compressional wave. R is always positive, so that waves with $n_\parallel^2 > 1$ are evanecent below a density such $\omega_{pi}^2/\Omega_{ci}^2 \simeq n_\parallel^2$.

In multispecies plasmas, S and L have a zero between each pair of cyclotron frequencies. The quantitative investigation of minority heating must therefore take into account the existence of a perpendicular resonance [3],

$$n_\perp^2 \to \infty \qquad \text{where} \qquad n_\parallel^2 = S \tag{3.18}$$

and an associated cut–off

$$n_\perp^2 = 0 \qquad \text{where} \qquad n_\parallel^2 = L \tag{3.19}$$

separated by a layer of evanescence. Since $n_\parallel^2 << \omega_{pi}^2/\Omega_{ci}^2$, these conditions can in practice be assimilated to $S = 0$ and $L = 0$ respectively; this allows to derive simple formulas for the position of the wave resonance and cut–off. Denoting with indexes M and m the majority and minority species, respectively, one finds:

$$\left.\frac{x}{R_o}\right)_S = \sqrt{\frac{1 + Z_m\nu_m\left(\frac{Z_M/A_M}{Z_m/A_m} - 1\right)}{1 + Z_m\nu_m\left(\frac{Z_m/A_m}{Z_M/A_M} - 1\right)}} - 1 \simeq \frac{1}{2} Z_m\nu_m\left(\frac{Z_M/A_M}{Z_m/A_m} - \frac{Z_m/A_m}{Z_M/A_M}\right) \tag{3.20}$$

$$\left.\frac{x}{R_o}\right)_L = Z_m\nu_m\left(\frac{Z_M/A_M}{Z_m/A_m} - 1\right) \tag{3.21}$$

where A_i, Z_i are the mass and charge numbers, and $\nu_i = n_i/n_e$ the concentrations; x is the horizontal distance from the position of the cyclotron resonance of the minority, R_o. Both the resonance and the cut–off are located between the cyclotron resonances of the two species, and approach the one of the minority, R_o, when the minority concentration tends to zero; thus they are both on the high magnetic field side if the charge–to–mass ratio Z/A of the minority is larger than that of the majority (e.g H^+ and He_3^{++} minorities in D^+), to the low field side in the opposite case (e.g. He_3^{++} minority in H^+); the cut–off is always to the outside.

When a fast wave is launched towards such a confluence, it will be partly reflected, partly transmitted, and partly absorbed. In a plane stratified model in which only the variation of B_o in the horizontal direction is taken into account, the cold plasma wave equations in the resonance region for $k_\parallel = 0$ can be cast in the form (Budden model, [32])

$$\frac{d^2}{dx^2}\left[\left(1 - \frac{x_S}{x}\right)E_+\right] + n_{\perp F}^2\left(1 - \frac{x_L}{x}\right)E_+ = 0 \tag{3.22}$$

where

$$n_{\perp F}^2 = -\frac{(n_\parallel^2 - R_D)(n_\parallel^2 - L_D)}{(n_\parallel^2 - S_D)} \tag{3.23}$$

is the FW perpendicular index of the pure majority plasma. A simple change of variable transforms this into a Whittaker equation (a particular case of the confluent hypergeometric equation), whose solutions satisfying the appropriate conditions at large distance

yield the coefficients of transmission and reflection. For a wave incident from the low magnetic field side one finds

$$R_+ = (1 - e^{-2\eta})^2 \qquad T_+ = e^{-2\eta} \tag{3.24}$$

and for a wave incident from the high magnetic field side

$$R_- = 0 \qquad T_- = e^{-2\eta} \tag{3.25}$$

where η is the optical thickness of the evanescence layer, evaluated with the perpendicular index of the FW in the absence of minority ions:

$$\eta = \frac{\pi}{4}\frac{\omega}{c}R_o\sqrt{\frac{(n_\parallel^2 - R_M)^3}{(n_\parallel^2 - S_M)^3(n_\parallel^2 - L_M)}\cdot\frac{\omega_{pm}^2}{\Omega_{cm}^2}} \tag{3.26}$$

R_M, L_M, S_M being the contribution of the majority ions to the corresponding elements of the cold dielectric tensor. Note that $R_\pm$ and $T_\pm$ do not add up to unity: the missing power, respectively

$$A_+ = e^{-2\eta}(1 - e^{-2\eta}) \qquad A_- = 1 - e^{-2\eta} \tag{3.27}$$

is interpreted as absorbed, in agreement with the fact that the group velocity tends to zero near the resonance. Absorption is more efficient for a wave incident from the high magnetic side, which encounters the resonance first.

Direct cyclotron damping on the minority species can be estimated by integrating the power balance equation (3.11) over the cyclotron resonance layer, where now the dominant contribution to the r.h. side,

$$\mathrm{Im}(L) = \sqrt{\pi}\frac{\omega_{pm}^2}{\Omega_{cm}^2}x_{om}e^{-x_{1m}^2} \tag{3.28}$$

is that of the minority, while the solution of the wave equation is used to relate $|E_+|^2$ to the incident flux. In this way it is found that

$$\frac{\Delta P_x}{P_x} \simeq \frac{\epsilon^{-1}}{1+\epsilon^{-1}}\left(\frac{\omega}{c}R\right)\left(\frac{\omega_{pM}^2}{\Omega_{cM}^2}\right)^{1/2}\nu_m \tag{3.29}$$

whith

$$\epsilon \simeq \alpha\left(n_\parallel^2\frac{v_{thm}^2}{c^2}\right)^{-1}\nu_m^2 \tag{3.30}$$

where $\alpha = O(1)$ depends on Z/A of the two species. $\Delta P_x/P_x$ is proportional to ν_m at very low concentrations ($\epsilon >> 1$), and inversely proportional to it in the opposite limit ($\epsilon << 1$), when screening becomes important again.

When finite electron inertia and/or finite temperature effects are taken into account, the FW resonance is replaced by confluence with a slower wave. Thus mode conversion is expected to play a central role also in ICR heating. Eq. (1.21) shows that the nature of the mode–converted wave depends on the ratio

$$\frac{P\sigma}{S} = O\left(\frac{m_i}{m_e}\beta\right) \tag{3.31}$$

If $\beta \gtrsim m_e/m_i$ (and even much lower near the IC first harmonic where σ is resonantly large, while S remains finite), the slow wave is the Ion Bernstein wave (1.22). When this very mild condition is satisfied, the strongly evanescent slow wave $n_\perp^2 = P$ can be factorised away by letting $-P \to \infty$ (zero electron inertia limit), so that the dispersion relation becomes:

$$-\sigma n_\perp^4 + \left[(n_\parallel^2 - S) + (n_\parallel^2 - R)\lambda + (n_\parallel^2 - L)\rho\right] n_\perp^2 + (n_\parallel^2 - R)(n_\parallel^2 - L) = 0 \tag{3.32}$$

Fig. 13 shows dispersion curves near the ion–ion resonance in the limit $k_\parallel = 0$, for a few values of the minority concentration. Confluence and cut–off are separated by a region of evanescence, as in the cold limit, except that its width δX does not shrink to zero in the limit $\nu_m \to 0$. δX and the corresponding optical thickness (defined again using the refractive index of the Fast Wave in the limit of cold majority alone) can be can be estimated from Eq. (1.21) with suitable approximations. For $\nu_H = 0$ one finds:

$$\frac{\delta X}{R_o} = 4\sqrt{3}\beta_D \qquad \eta_D = \frac{\pi}{2}\frac{\omega}{c}R_o\left(\frac{\omega_{pD}^2}{\Omega_{cD}^2}\right)^{1/2}\beta_D \tag{3.33}$$

As soon as $\nu_H \gtrsim \beta_D$, on the other hand, δX is determined mainly by the minority ions, and includes, in addition to the zone where the two roots are complex conjugate, also the region extending to the $L = 0$ cut–off:

$$\frac{\delta X}{R_o} = \frac{3\sqrt{3}}{2}\nu_H\left(\frac{\nu_H}{\beta_D}\right)^{1/2} \qquad \eta_H = \frac{\pi}{2}\frac{\omega}{c}R_o\left(\frac{\omega_{pD}^2}{\Omega_{cD}^2}\right)^{1/2}\nu_H \tag{3.34}$$

A quantitative evaluation of mode conversion requires the solution of a wave equation taking into account the finite temperature corrections just discussed. The differential form of these additional terms cannot be determined unambiguously with elementary

considerations, however, and has been obtained only relatively recently by Swanson [34] and by Colestock and Kashuba [35] by expanding in powers of the ion Larmor radius the solution of Vlasov equation in a non–uniform magnetic field. The finite Larmor radius (FLR) wave equation thus obtained has been solved analytically in a few limiting cases (pure first harmonic heating, and $\nu_m \gg \beta_M$, both with $k_\parallel = 0$, [36]), and numerically. The results suggest that for small $k_\parallel$ Eqs. (3.24–27) still hold, if $\eta \simeq \eta_D + \eta_H$, and $A_\pm$ is interpreted as the fraction of power which is mode converted to the IBW. This power is thought to be finally damped on the electrons; this is not predicted by the linear theory (cfr. below), but is in agreement with the direct electron heating seen in the experiments under conditions of efficient mode conversion.

At large values of $k_\parallel$ the dispersion curves are modified by cyclotron damping, as shown in Fig. 14. If the width of the absorption region extends to the evanescence region, the confluence is washed out, and the efficiency of mode conversion is drastically reduced. The critical value of $k_\parallel$ can be obtained by comparing $(\Delta x)_{Res}$ with x_S:

$$|n_\parallel|_c \frac{v_{thD}}{c} \simeq \beta_D \tag{3.35}$$

in the case of first harmonic heating, and

$$|n_\parallel|_c \frac{v_{thH}}{c} \simeq \frac{3}{8}\nu_H \tag{3.36}$$

in the case of minority heating. The last equation is often used, for a given $n_\parallel$, to define a critical H^+ concentration below which absorption will be dominated by cyclotron damping on the minority ions ("minority" regime); above this critical concentration on the other hand mode conversion will be predominant ("mode conversion" regime). The best absorption occurs always well in the minority regime. In practice however the concentration is fixed, while the $k_\parallel$–spectrum excited is broad: conditions (3.31) should be interpreted as separating the low $k_\parallel$ part which is predominantly mode–converted, from the large $k_\parallel$ part which is mostly absorbed directly by cyclotron damping. The relative weight of the two damping mechanisms can be influenced by shaping the spectrum (cfr. below).

In scenarios where the cyclotron resonance of the minority ions does not coincide with the first harmonic of the majority, the details of the dispersion curves near the associated ion–ion resonance are more complicated. In this case FLR terms are not resonant, hence much smaller than in the H^+ in D^+ case. Whether FLR or finite electron inertia corrections are more important depends then on wether β is larger or

smaller than m_e/m_i. In tokamaks, the former is usually the case, so that one would again predict confluence with the pressure–driven wave (1.22), rather than with the cold ion cyclotron wave (1.16). However, the wavelength predicted by (1.22) are so short that the condition $k_\perp \rho_i << 1$ is violated: under this condition Eq. (1.22) itself is no more reliable, and one should solve the complete hot–plasma dispersion relation. Moreover, one can argue that in this case the poloidal component of the static magnetic field could also play a role.

In practice however this discussion is pointless. Because of the smallness of the FLR corrections, the resonance of the fast wave is so sharp that residual cyclotron damping by the minority ions, or even the very weak collisional damping, is sufficient to wash out completely the confluence. Ion–ion resonances of this kind (which we propose to call "non–degenerate") are to all purpose really cold plasma resonances, as described by the Budden model. Examples of "exact" dispersion curves for the case of He_3^{++} in H^+ are shown in Fig. 15. The electric field pattern in the vicinity of $x = x_S$ obtained by solving the FLR wave equations numerically is dominated by the logarithmic singularity associated with the wave resonance.

Let us finally exhamine in some more details the properties of the slow cold plasma wave in the IC frequency domain. Taking into account that $|P|$ is m_i/m_e times larger than the other elements of the dielectric tensor, the only possibility to satisfy Eq. (1.16) is to choose $n_\parallel^2$ so that

$$n_\parallel^2 = S \tag{3.37}$$

In the MHD limit, this is the dispersion relation of the shear Alfvén wave. In the ion cyclotron range this wave is known as the ion cyclotron wave, and suffers a parallel resonance, $k_\parallel \to \infty$ as the frequency approaches Ω_{ci}. Thus it can be excited only at magnetic fields higher than the resonant value, and the launcing structure must impose a very short parallel wavelength to match (3.37). These properties have been exploited in the well–known magnetic beach concept by Stix [37]. In a tokamak however there is no possibility of launching this wave from the outside.

When (3.37) is not satisfied, the dispersion relation of the slow wave reduces to

$$n_\perp^2 = P \tag{3.38}$$

Under normal conditions ($\omega/k_\parallel v_{the} >> 1$), this represents an evanescent wave with extremely short evanescence length. For most purposes, as already mentioned, it can be factorised away from the dispersion relation by letting $m_e/m_i \to 0$. In this limit,

the plasma is a perfect conductor along magnetic field lines, as in ideal MHD. At the plasma–vacuum boundary, the evanescent wave (3.38) is then replaced by image surface currents which screen any h.f. poloidal magnetic field from the plasma interior. To avoid dissipation associated with these surface currents, the parallel component of the electric field in vacuum is often suppresseded using an anisotropic Faraday screen, made of conducting rods aligned with the static magnetic field. If the condition $\omega/k_{\|} v_{the} \lesssim 1$ is satisfied, the slow wave becomes again propagative, but is then heavily damped on the electrons. This situation is however unlikely to occur in the cool outer layers of the plasma.

3.3 - Fast Wave coupling. The natural candidate to implement ICRH in tokamaks is clearly the fast wave. Let us now consider its coupling and propagation from the plasma perifery to the absorption region. To launch this wave, an oscillating magnetic field parallel to the static one must be excited. The most convenient launching structure is therefore a metallic antenna, oriented so that the current flows in the poloidal direction. Using multiple loop antennas and phasing the single conductors, spectral shaping can be achieved.

If for simplicity the antenna is considered infinitely long in the poloidal direction, the power per unit area radiated on the partial wave with toroidal wavenumber n_ϕ can be written as [38]

$$P(n_\phi) = Cte \cdot |J(n_\phi)|^2 \frac{\sinh^2 \nu_x (w-a)}{\cosh^2 \nu_x w} \frac{\mathrm{Re}\{Y(n_\phi)\}}{\left|\nu_x^2 - iY(n_\phi)\tanh \nu_x w\right|^2} \tag{3.39}$$

Here $J(n_\phi)$ is the toroidal Fourier transform of the antenna current, and $Y(n_\phi)$ the surface admittance of the plasma, defined as

$$Y(n_\phi) = \frac{B_z}{E_y} \tag{3.40}$$

for the wave with parallel wavenumber $k_{\|} \simeq n_\phi/R$ satisfying the outward radiation condition at high density (here it is assumed that corrections to $k_{\|}$ due to the poloidal magnetic field of the tokamak can be neglected in the near field region). The other factors take into account propagation in vacuum (the antenna is at a distance a, the metallic wall at a distance w from the plasma surface); $\nu_x^2 = n_{\|}^2 - 1$ is supposed positive, i.e. (3.39) is written for a wave evanescent in vacuum. Summing over n_ϕ and dividing by the square of the total current I_a flowing in the antenna one obtains the radiation resistance per unit length in the poloidal direction.

The surface admittance $Y(n_\phi)$ must be evaluated numerically. The main properties of Eq. (3.39) can however be easily understood by noting first of all that the width w_a of the conductors (10 to 30 cm) is necessarily much smaller than the vacuum wavelength; as a consequence, the factor $|J(n_\phi)|^2$ is very broad, its main peak extending to values of n_ϕ corresponding to $n_\parallel \simeq c/\omega w_a \gg 1$. The waves must however first tunnel to the cut–off $R = n_\parallel^2$: this filters out effectively waves whith too large $n_\parallel$, for which the evanescence layer in vacuum and at the plasma periphery is optically thick. Typical spectra for a two conductor antenna in the symmetric and antisymmetric configuration respectively are shown in Fig. 16 and 17.

The fact that the width of the radiated spectrum is determined partly by tunneling rather than by the antenna geometry alone has important consequences. First, to achieve a good radiation resistance the antenna should be as wide as compatible with the available access, and must be placed as close as possible to the plasma. The decrease of loading when the plasma moves away from the antenna is well–known to experimentalists. Secondly, the flexibility of spectral shaping is somewhat restricted: indeed, one cannot hope to achieve fine tuning of the spectrum with a coupling structure much shorter than one wavelength. In particular, an antisymmetric antenna often has an appreciably lower radiation resistance than a symmetric one: to locate the maximum of $|J(n_\phi)|^2$ within the domain of good tunneling requires rather broad conductors, which can be used only in devices with wide access ports.

Although predicting a loading resistance in reasonable agrement with the measured one, the above model of IC antennas is very rough. In the first place, one has to take into account that the antenna has a finite length in the poloidal direction, which is again usually small compared to the wavelength in vacuum. For this purpose, it is necessary to know the poloidal distribution of the current in the antenna. The usual method consists in treating each antenna conductor as a piece of transmission line, with appropriate boundary conditions at feeders and shorts [39]. In principle however the antenna current should be evaluated self–consistently: an elegant variational method for this purpose has been developed by Teilhaber and Jacquinot [40].

In the second place, the definition (3.40) of the surface impedance assumes that once the wave has reached a density sufficient for the validity of the WKB approximation it is never reflected back again towards the antenna. This requires a strong single transit absorption, which is by no means always guaranteed. If damping is weak, reflection from the opposite wall (or in the mode conversion regime, from the cut–off associated to the ion–ion resonance) gives rise to standing waves. The plasma filled vessel can

then be regarded as a cavity, possessing eigenmodes with a relatively large quality factor. Under these conditions, the level of excitation of individual n_ϕ modes by the antenna will depend on how well they match one of the possible eigenmodes. The power spectrum, which can be evaluated only by solving the wave equations through the whole plasma numerically, has then a typical line structure (Fig. 18). Note however that its overall width is unchanged: as a consequence several eigenmodes can be simultaneously excited. If the plasma parameters vary slightly, the corresponding peaks in the spectrum will just move around a little, without sharp effects on the global loading. Nevertheless a scan of the radiation resistance versus static magnetic field (Fig. 19) shows that loading peaks occur when an eigenmode corresponds to values of $n_\parallel$ close to unity. The reality of these loading resonances has recently been confirmed in JET. The results of Figs. 16–19 have been obtained with a Finite Element code which solves the FLR wave equations in a plane stratified model of the tokamak, in which curvature and shear are neglected.

3.4 - Heating with Bernstein waves. Direct launching of Bernstein waves has been proposed as a viable alternative to fast wave launching, and has been successfully tested in several moderate power experiments. Here we will comment very briefly on this heating scheme (for a review, cfr. [41]).

Bernstein waves are hot plasma waves associated with the harmonics of the ion cyclotron frequency. Because of their large perpendicular index, their properties are usually investigated in the electrostatic approximation, $\epsilon_{xx} n_\perp^2 + \epsilon_{zz} n_\parallel^2 = 0$ (cfr. Eq. 1.8). Expanding the full dispersion relation in powers of n^{-2} shows however that the first electromagnetic corrections cancel the last term, so that the correct dispersion relation is simply [42]:

$$\epsilon_{xx} = 1 - \sum_j \frac{\omega_{pj}}{\omega^2} \sum_{n=-\infty}^{+\infty} \frac{n^2}{\lambda_j} I_n(\lambda_j) e^{-\lambda_j} \left(-x_{0j} Z(x_{nj})\right) = 0 \qquad (3.41)$$

The lowest IBW has already been discussed at length above in connection with mode conversion; higher order BWs are of correspondingly higher order in $k_\perp^2 v_{thi}^2 / \Omega_{ci}^2$.

According to Eq. (3.41), Bernstein waves are subject to strong ion cyclotron damping in the vicinity of ion cyclotron harmonics. On the other hand, the parallel electric field is much smaller than predicted by the electrostatic approximation; as a consequence damping of BW by the electrons is very weak, since neither Transit Time nor Landau absorption can occur to lowest order. This allows good penetration even in

high temperature plasmas. In the experiments, absorption by ions appears to take place also near half–harmonics of the cyclotron frequency [43], [44]: this is attributed to parametric decay processes, or possibly to stochastic ion heating.

An advantage of IBWH is that in sufficiently large devices BW waves could also be launched with waveguides (at least two are needed to produce an antisymmetric spectre, cfr. below). A complete theory of coupling to BW exists however only for the lowest one, for which the FLR wave equations derived in [34]–[35] can be used [42]. To launch this wave with a metallic antenna, the conductors must be oriented so that the current flows parallel to the static magnetic field. This immediately shows that to achieve good coupling the plasma density in the vicinity of the antenna should be low, otherwise this current will be competely screened by currents on the surface of the plasma (in practice, a density not exceeding a few times 10^{11} cm^{-3} is adequate). On the other hand the loading resistance will not drop dramatically if the plasma shifts away from the antenna. Secondly, since coupling is ensured by E_z, which is proportional to $k_{\|}$ (crf. Eq. (3.16), which is valid also for these waves), the antenna must be antisymmetric: e.g. a T–antenna with feeder at the center and with shorts at the ends, or two guides excited in opposition. Finally, although the lowest BW exists throughout the frequency range between Ω_{ci} and $2\Omega_{ci}$, good loading is found only when the first harmonic is just behind the antenna (Fig. 20), so that the difference between the wavelength in vacuum and in the plasma is not extremely large. The need to match the applied frequency to the edge magnetic field limits somewhat the flexibility of IBW antennas.

3.5 - Global solutions of the wave equations in Tokamaks. The effects of toroidicity on the propagation of h.f. waves in the IC frequency range are even more important than in the LH case. Ray Tracing has been used also in this domain [25]: although it is only justified in very large plasmas (JET or bigger), it is fast, and can easily deal with general equilibria (non–circular, high β, etc). Coupled with a fast code evaluating the antenna, and with a one–dimensional treatment of mode conversion and absorption in the resonance regions, Ray Tracing provides a rapid and reliable estimate of first transit absorption. This also immediately points out its main limitation, namely its inability to give a complete picture of what happens when absorption is weak and global eigenmodes are excited.

The numeric solution of Maxwell equations in tokamak geometry is a difficult problem for two reasons. First, because of parallel dispersion (of which cyclotron damping is a consequence) the the h.f. current is a non–local function of the wave electric field.

Since the tokamak does not posses translational symmetry along magnetic field lines, it is not possible to transform this integral relation into an algebraic one using a Fourier transformation, as in slab geometry. As a consequence, one has to solve a system of integro–differential equations. Secondly, the need to resolve short wavelength Bernstein waves puts extremely severe requirements on the mesh to be used.

The first attempts to global numerical solutions where based on the cold plasma approximation, and used suitably enhanced collisions to smooth the singularities at ion–ion resonances (for a review, cfr [46]). This procedure of course eliminates mode conversion and cyclotron damping. The first hot plasma codes neglected the poloidal magnetic field [47], or made use of a method known as "order reduction" to take into account FLR effects on the Fast Wave (including depletion by mode conversion), while eliminating the short wavelength BW from the solution [48]. Both these approaches avoid the difficulties mentioned above. While the cold model is too crude to be really useful, and can be even misleading, the "mode reduction" approach is likely to give excellent results.

A code which solves the full integro–differential FLR wave equations in tokamak geometry (although only with circular cross–section) has recently been developed by Krücken and myself [49]. To cope with the integral operators of the constitutive relation, we have used a semispectral approach, expanding the solution in poloidal Fourier modes, and using cubic Hermite Finite elements in the radial direction. Poloidal modes are not even approximately eigenmodes, so that a large number is needed to ensure convergence. This unfortunately puts an upper limit to the size of the plasma which can be simulated: when BW are excited, ASDEX is close to this limit. On the other hand convergence is robust, and BW can nicely be resolved.

A global code of this kind requires large amounts of computer time, and is therefore hardly suited for parameter studies: its natural use is to test the validity of our ideas about mode conversion and absorption, and to benchmark simpler models such as Ray Tracing, or the plane–stratified code mentioned above. Two examples of such a comparison is given in Fig. 21, showing the n_ϕ–power spectrum coupled in the case of first harmonic heating of Deuterium and in the case of 5 % H^+ minority heating in ASDEX. The former is a weak single–pass absorption scenario: both codes predict the excitation of eigenmodes. In the second case the temperature was taken to be higher because the plasma was pre–heated by neytral beam injrction; single pass absorption is therefore large, and eigenmodes are not excited. In view of the different geometry, agreement is

surprisingly good. In the high absorption case, Ray Tracing can also be quantitatively trusted (fig. 22).

The most significant discrepancies between the one–dimensional and fully toroidal simulations concern, not astonishingly, the behaviour of Bernstein waves: the efficiency of mode conversion is considerably reduced by toroidicity. This can be easily understood by noting that the integral operators describing parallel dispersion are in this respect equivalent to a quite strong broadening of the $k_{\|}$–spectrum. Thus even the $n_\phi = 0$ toroidal mode, which in the slab limit has $k_{\|} = 0$ and is strictly in the mode–conversion regime, in toroidal geometry suffers severe cyclotron damping. Not foreseen was the fact that BW are found to propagate away from the mode conversion layer with essentially vertical wavefronts (Fig. 23). As expected, they are rather weakly damped by the electrons, so that it has proved necessary to introduce an 'ad–hoc" damping where their wavelength becomes comparable with the ion Larmor radius: otherwise they are finally damped numerically, making it impossible to check the global power balance. Although such ad–hoc damping lacks theoretical justification, it is a fair phenomenologic description of what is observed experimentally.

3.6 - Conclusions. ICRH has proved very successful, and there is every reason to believe that it will remain so in reactor–grade plasmas. The status of ICRH theory can be considered satisfactory: the basic mechanisms of coupling, propagation and absorption are well understood, and modeling has recently improved to the point of including also fine effects such as the influence of toroidicity on mode conversion. Among the points which require further investigation, we can mention the details of absorption of Bernstein waves, the effects of ICR heating on particle and energy lifetimes, the mechanisms of impurity production during high power experiments, and more generally the interactions of the h.f. fields with the scrape–off plasma. Not clear is also whether current drive is possible at these frequencies with sufficient efficiency.

REFERENCES.

[1] T.H. Stix, *The theory of plasma waves*, McGraw–Hill (N.Y.), 1961.

[2] B.D. Fried, S.D. Conte, *The plasma dispersion function*, Academic Press (N.Y.), 1961

[3] S.J. Buchsbaum, Phys. Fluids **3** (1960) 418.

[4] M. Brambilla, Plasma Phys. **18** (1976) 669.

[5] V.E. Zacharov, V.I. Karpman, Sov. Phys. JETP 16 (1963) 351.

[6] E. Canobbio, Nucl. Fusion 12 (1972) 561.

[7] A.A. Vedenov, E.P. Velikhov, R.Z. Sagdeev, Nucl. Fusion 1 (1961) 82.

[8] W.E. Drummond, D. Pines, Nucl. Fusion Suppl. Pt. 2 (1962) 465.

[9] C.F. Kennel, F. Engelmann, Phys. Fluids 9 (1966) 2377.

[10] T.H. Stix, Phys. Rev. Lett. **15** (1965) 878.

[11] C.F.F. Karney, Phys. Fluids **21** (1978) 1584.

[12] C.F.F. Karney, Phys. Fluids **22** (1979) 2188.

[13] M. Brambilla, Yang–Ping Chen Nucl. Fus. **32** (1983) 541.

[14] N.J. Fish, Phys. Rev. Lett. **41** (1979) 873.

[15] N.J. Fish, Rev. Mod. Phys **59** (1987) 175.

[16] F. Leuterer et al., 13th Eur. Conf. on Controlled Fusion and Plasma Heating, Schliersee 1986, Vol. 2 p. 409.

[17] J.E. Stevens, R.E. Bell, S. Bernabei et al., Nucl. Fus. **28** (1988) 217.

[18] P. Lallia, 2d Top. Conf. on R.F. Plasma Heating, Lubbock (Texas) 1974, paper C3.

[19] M. Brambilla, Nucl. Fus. **16** (1976) 47.

[20] V.E. Golant, Sov. Phys. Tech. Phys. **16** (1972) 1980.

[21] H.H. Kuehl, Phys. Fluids **5** (1962) 1095.

[22] P.M. Bellan, M. Porkolab, Phys. Fluids **17** (1974) 1592.

[23] I.B. Bernstein, Phys. Fluids **18** (1975) 320.

[24] M. Brambilla, A. Cardinale Plasma Physics **24** (1982) 1187.

[25] M. Brambilla, Comp. Phys. Rep. **4** (1986) 71.

[26] P.T. Bonoli, R.C. Englade, Phys. Fluids **29** (1986) 2937.

[27] T.H. Stix, Course and Workshop on Applications of RF power to Tokamak plasmas (EUR-10333-EN), Varenna 1985, Vol. 2 p. 24.

[28] V.L. Vdovin et al., 3d Int. Symp. on Heating in Toroidal Plasmas, Grenoble 1976, Vol 2., p. 349.

[29] J. Adam, A. Samain, Report EUR-CEA-FCV 579 (1971), Fontenay–aux–Roses.

[30] J.C. Hosea et al., 8th IAEA Conf. on Plasma Physics and Contr. Fusion Res., Bruxelles 1980, Vol. 2 p. 95.

[31] T.H. Stix, Nucl. Fus. **15** (1975) 737.

[32] K.G. Budden, *Radiowaves in the ionosphere*, Cambridge Univ. Press 1961, Ch. 21.

[33] R.R. Weynants, Phys. Rev. Lett. **33** (1974) 78.

[34] D.G. Swanson, Phys. Fluids **24** (1981) 2035.

[35] P.L. Colestock, R. Kashuba, Nucl. Fus. **13** (1983) 763.

[36] M. Brambilla, M. Ottaviani, Plasma Phys. Contr. Fus. **27** (1985) 1.

[37] T.H. Stix, Phys. Fluids **1** (1958) 308.

[38] V.P. Bhatnagar et al., 2d Int. Symp. on Heating in Toroidal Plasmas (EUR-7424-EN), Como 1980, Vol. 1 p. 561.

[39] V.P. Bhatnagar et al., Nucl. Fus. **22** (1982) 279.

[40] K. Teilhaber, J. Jacquinot, Nucl. Fus. **24** (1984) 541.

[41] M. Ono, Course and Workshop on Applications of RF power to Tokamak plasmas (EUR-10333-EN), Varenna 1985, Vol. 2 p. 197.

[42] M. Brambilla, Nucl. Fus. **28** (1988) 549.

[43] J. Moody et al., Phys. Rev. Lett. **60** (1988) 298.

[44] M. Ono et al., Phys. Rev. Lett. **60** (1988) 294.

[45] K. Steinmetz et al., 11th IAEA Conf. on Plasma Physics and Contr. Fusion Res., Kyoti 1986, Vol. 1 p. 461.

[46] L. Villard et al., Comp. Phys. Rep. **4** (1986) 95.

[47] A. Fukuyama et al., Comp. Phys. Rep. **4** (1986) 137.

[48] D.N. Smithe et al., Nucl. Fus. **27** (1987) 1319.

[49] M. Brambilla, T. Krücken, submitted for publication.

FIGURE CAPTIONS.

Fig. 1 - Exact dispersion curves near the LTP (in the electrostatic approximation). Deuterium plasma, $n_{\|} = 1.8$.

Fig. 2 - Sketch of the ion resonance with a LH wave propagating in the x–direction.

Fig. 3 - Diffusion coefficient for Stochastic Ion Heating by a plane LH wave.

Fig. 4 - Damping a LH wave by perpendicular ion Landau Damping, as a function of applied power. The plasma parameters are those of the ASDEX LH experiment [40].

Fig. 5 - Quasilinear plateau formation in thr electron distribution function.

Fig. 6 - Schematic dispersion curves illustrating the accessibility condition ($y^2 = \omega^2/\Omega_{ci}\Omega_{ce}$).

Fig. 7 - Total energy reflection coefficient in the ASDEX 8–waveguide Grill ($f = 1.3$ Ghz, $b = 2.1$ cm) versus $\Delta\Phi$ for a few values of the edge profile parameters ($n_e(0)$, cm^{-3} and $dn_e/dx)_o$, cm^{-4}, are assumed numerically equal).

Fig. 8 - Total energy reflection coefficient in the ASDEX 8–waveguide Grill at $\Delta\Phi = 90^o$ and $\Delta\Phi = 180^o$, versus the edge density, for different values of the edge density gradient.

Fig. 9 - Power spectra of the Asdex 8-waveguide Grill for different values of $\Delta\Phi$.

Fig. 10 - Ray tracing: projection of the central rays from the Grill in the poloidal plane (dots are 5 wavelengths apart) for a typical ASDEX Lower Hybrid case ($R =$ 1.65m, $a = 0.4$ m; $B_o = 2.2$ T; $n_e(0) = 6\ 10^{13}$ cm^{-3}; $T_e(0) = 0.6$ keV; $T_i(0) = 0.55$ keV).

Fig. 11 - Ray tracing: evolution of $n_{\|}$ along the rays.

Fig. 12 - Ray tracing: evolution of $n_{\perp}$ along the rays.

Fig. 13 - Dispersion curves near $\omega = 2\Omega_{cD}$ for perpendicular propagation in a D-H plasma (Jet–like parameters: R = 300 cm, $B_o = 2.7$ T, $n_e = 6\,10^{13}$ cm^{-3}, T = 2 keV).

Fig. 14 - Dispersion curves near $\omega = 2\Omega_{cD}$ in pure D^+, $n_{\|} = 3$.

Fig. 15 - Dispersion curves near $\omega = \Omega_{cHe}$; 0.5 % He_3^{++} in a Hydrogen plasma.

Fig. 16 - Power spectrum from a two conductor antenna (widh of each conductor 14 cm, gap 10 cm) in the symmetric configuration, outward radiation conditions at 30 cm from the plasma edge. The parameters are those of the ASDEX ICRH experiment [45] ($f = 33.5$ Mhz, 5 % H^+ in D^+; $T_D(0) = 2.2$ keV, $T_H(0) = 4.4$ keV).

Fig. 17 - Power spectrum from the antisymmetric configuration of the same antenna, outward radiation conditions.

Fig. 18 - Power spectrum for D^+ first harmonic heating, symmetric configuration, taking into account reflection from the opposite wall.

Fig. 19 - Magnetic field scan of the 1–dim. FELICE code with reflection at the inner wall, showing eigenmodes. ASDEX parameters at 67 Mhz (first harmonic of H^+): a) Radiation resistance; b) Power balance.

Fig. 20. - Loop antenna launching of IB waves (parameters of the ALCATOR-C IBWH experiment, [43]). a) Radiation resistance versus magnetic field ($\omega/\Omega_{ci} = 2$ at the plasma edge when $B = 7.18$ T). b) fraction radiated into the BW, the FW, or absorbed in the near–field layer.

Fig. 21 - Power spectrum according to the fully toroidal simulation, compared to the one predicted by the plane–stratified model. ASDEX, a) first harmonic heating of Deuterium; b) 5 % H^+ in D^+.

Fig. 22 - a) Contour lines of E_x (horizontal component of the electric field) for the $n_\phi = 2$ mode of Fig. 21 a); b) E_+ in the equatorial plane for the same mode, showing the Bernstein waves to the left of the magnetic axis.

Fig. 23 - a) Countour lines of $\mathrm{Im}(E_y)$ for the $n_\phi = 16$ mode of fig. 21 b); b) wave–fronts according to ray tracing for the same case.

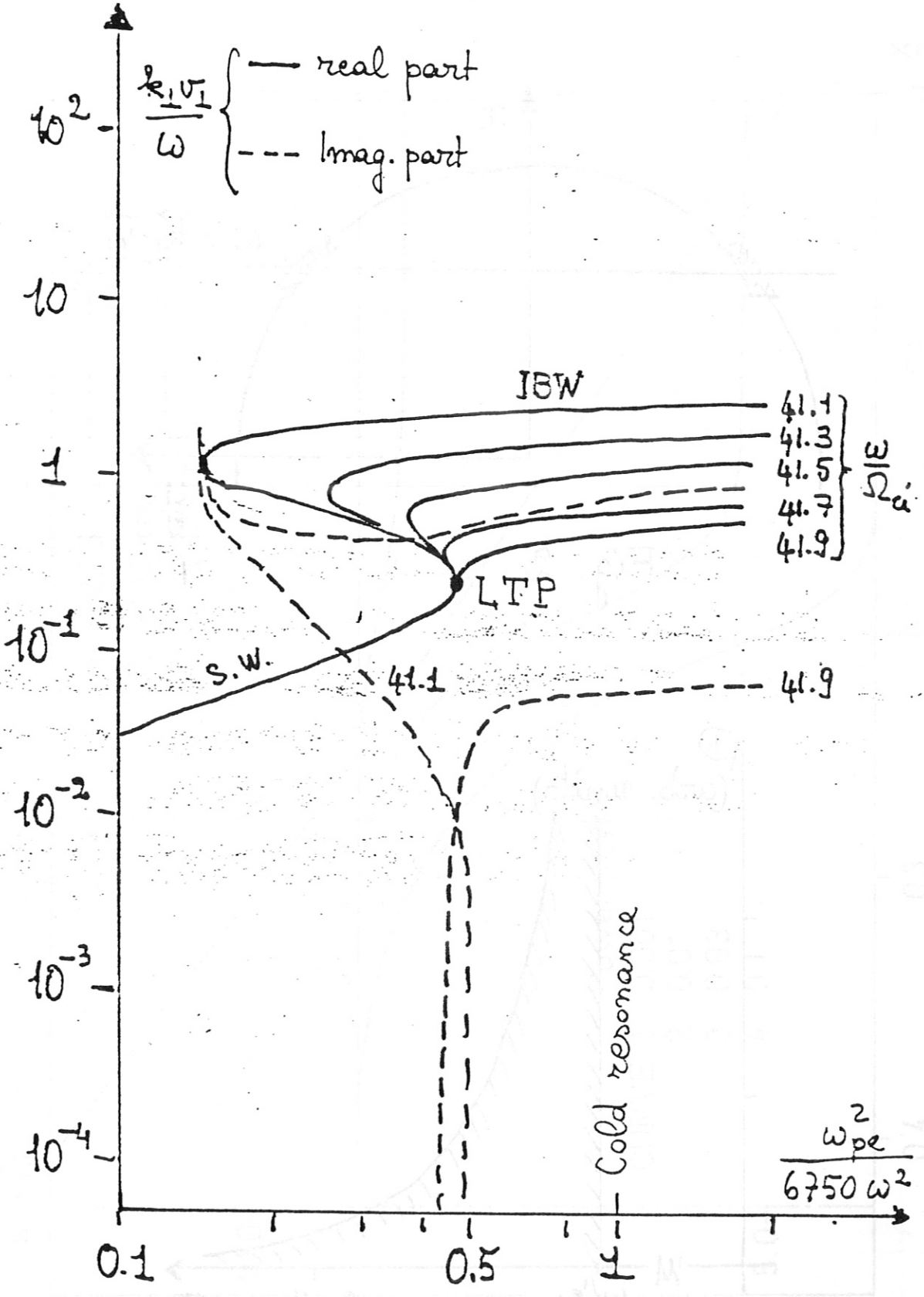
$\frac{k_\perp v_i}{\omega}$
real part
Imag. part
10^2
10
1
10^{-1}
10^{-2}
10^{-3}
10^{-4}
IBW
41.1
41.3
41.5
41.7
41.9
$\frac{\omega}{\Omega_i}$
LTP
S.W.
41.1
41.9
Cold resonance
$\frac{\omega_{pe}^2}{6750\,\omega^2}$
0.1
0.5
1

Fig. 1

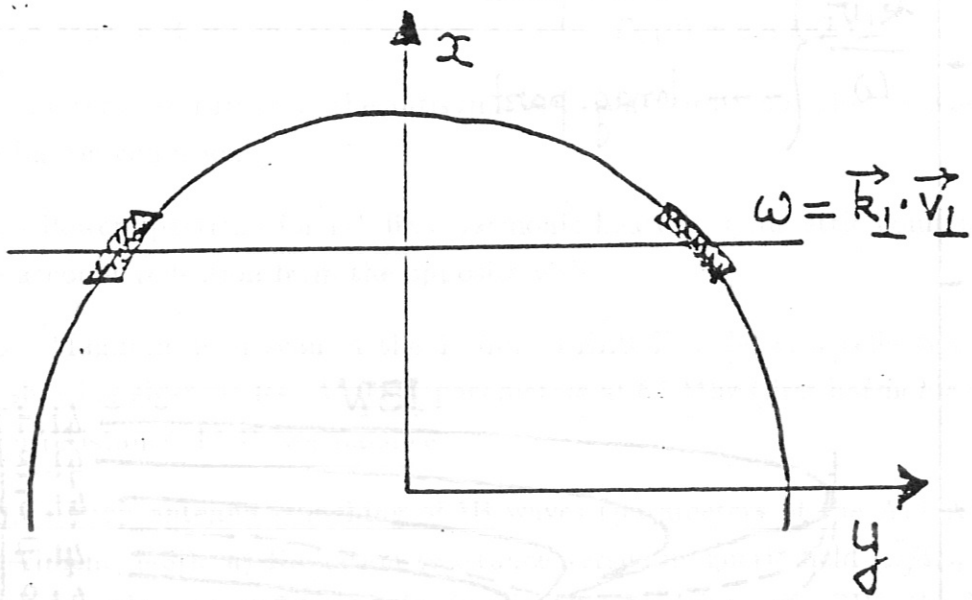
x
$\omega = \vec{k}_\perp \cdot \vec{v}_\perp$
y

Fig. 2

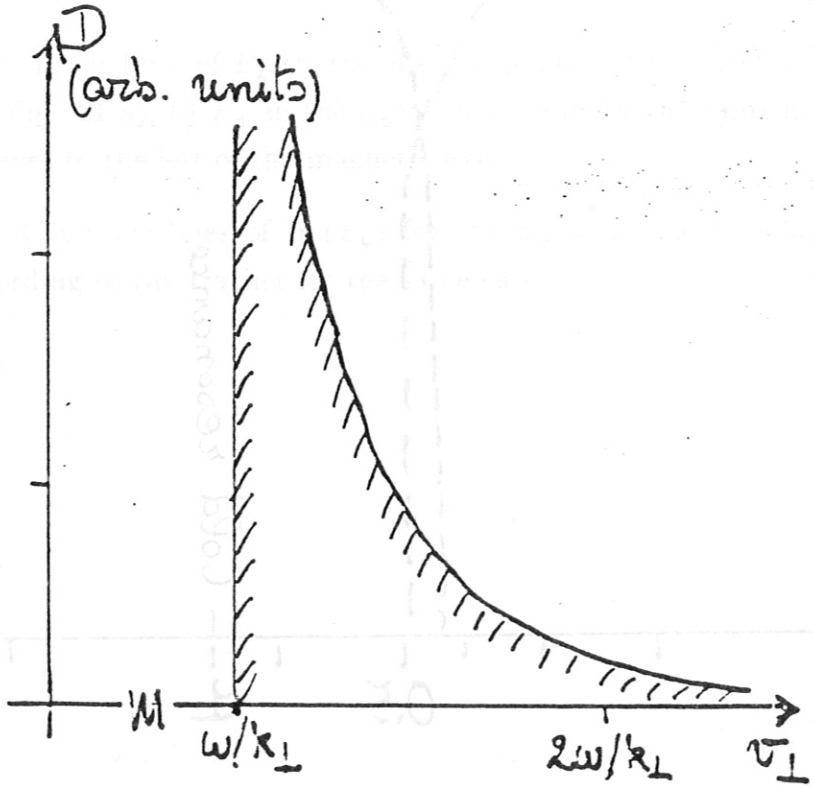
D
(arb. units)
M
$\omega/k_\perp$
$2\omega/k_\perp$
$v_\perp$

FIG. 3

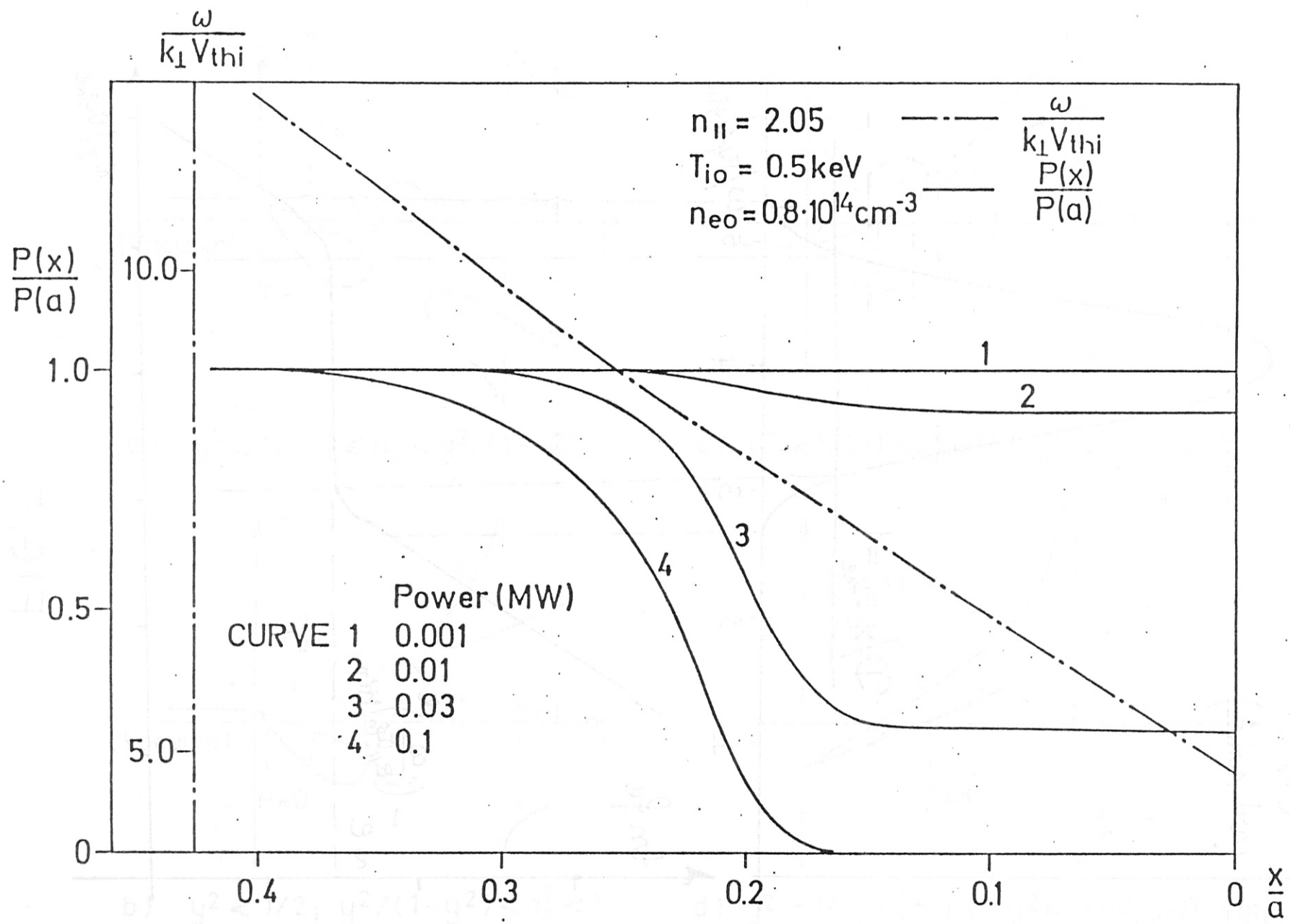
ω / k⊥ Vthi
n∥ = 2.05
Tio = 0.5 keV
neo = 0.8·10^14 cm^-3
ω / k⊥ Vthi
P(x) / P(a)
P(x) / P(a)
10.0
1.0
0.5
5.0
0
1
2
3
4
Power (MW)
CURVE 1 0.001
2 0.01
3 0.03
4 0.1
0.4
0.3
0.2
0.1
0
x / a

FIG. 4

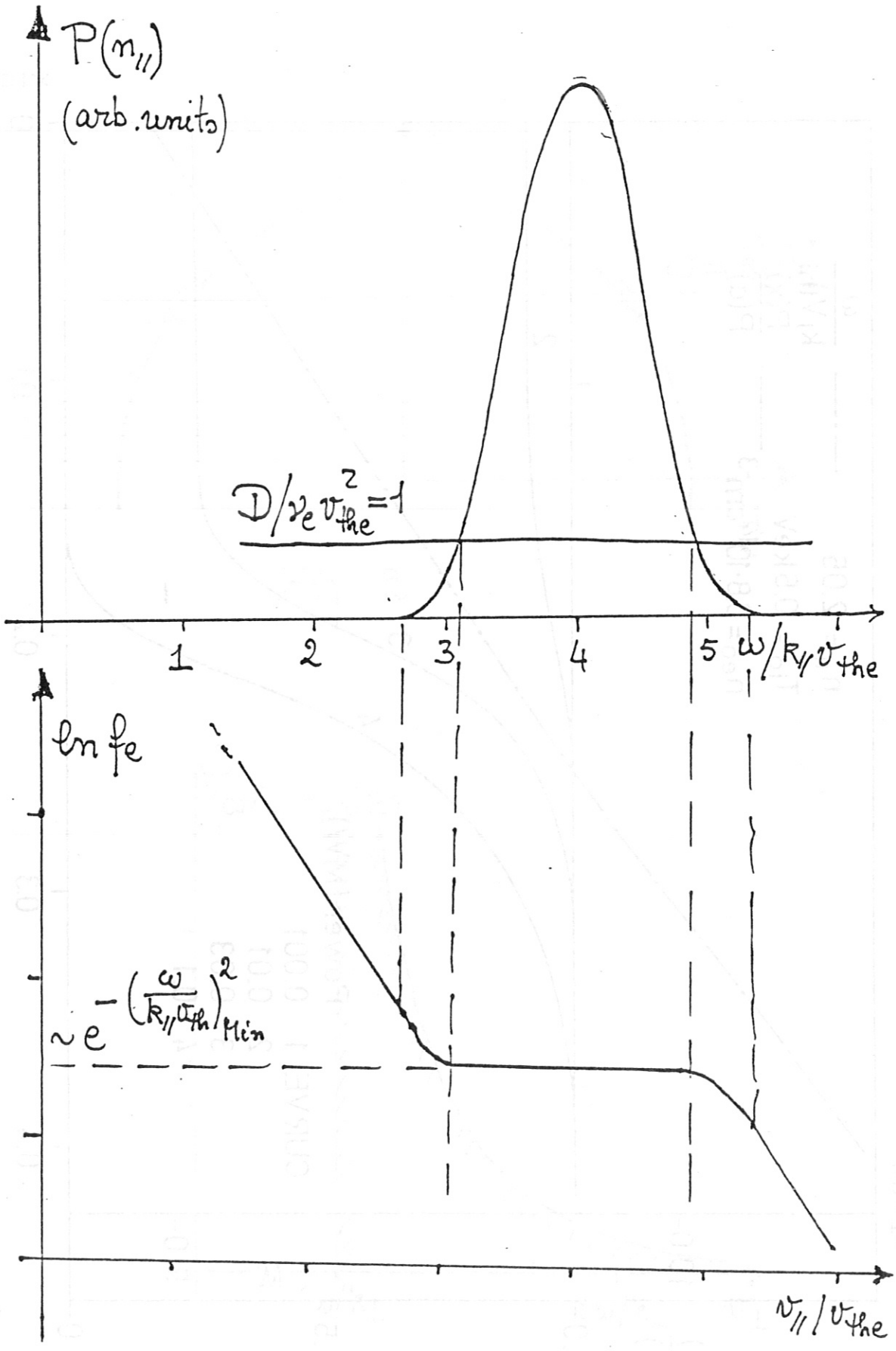

FIG. 5

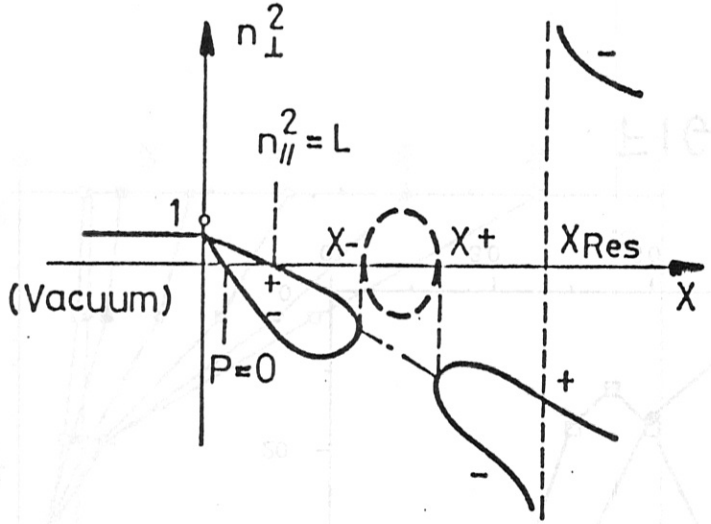

a) $y^2 < 1/2 ; 0 \leq n_{//}^2 < y^2/(1-y^2)$

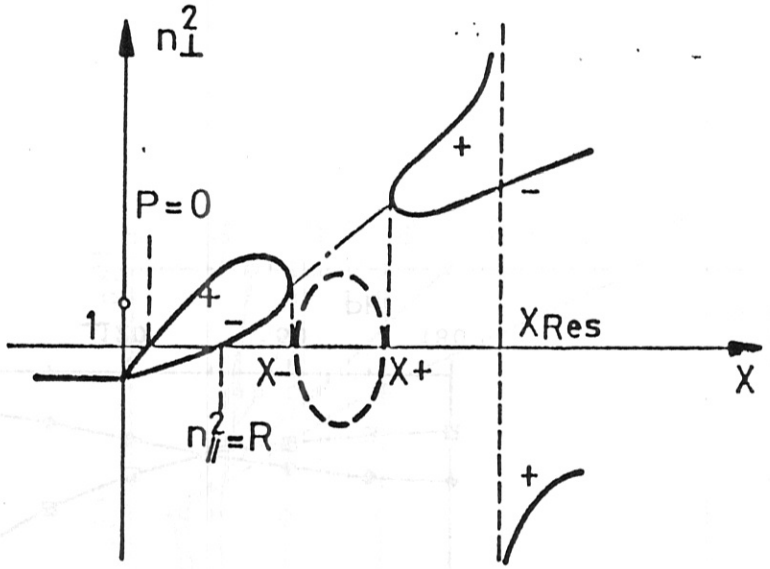

c) $y^2 < 1/2 ; 1 < n_{//}^2 < 1/(1-y^2) = 1 + (\omega_{Pe}^2/\Omega_{ce}^2)_{Res}$

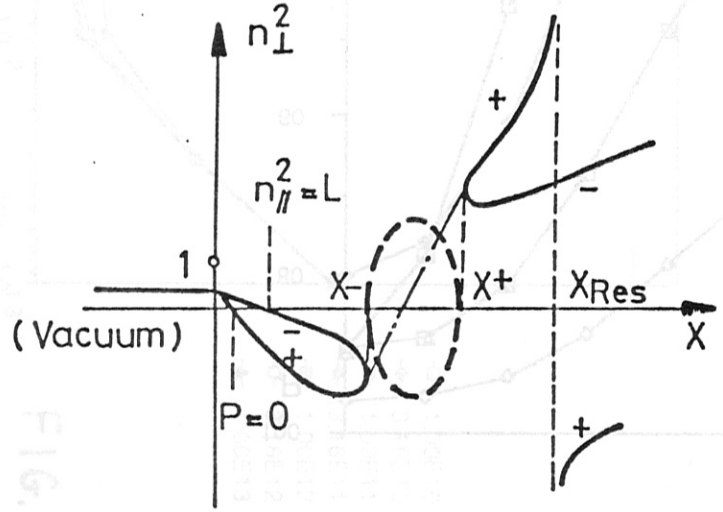

b) $y^2 < 1/2 ; \; y^2/(1-y^2) < n_{//}^2 < 1$

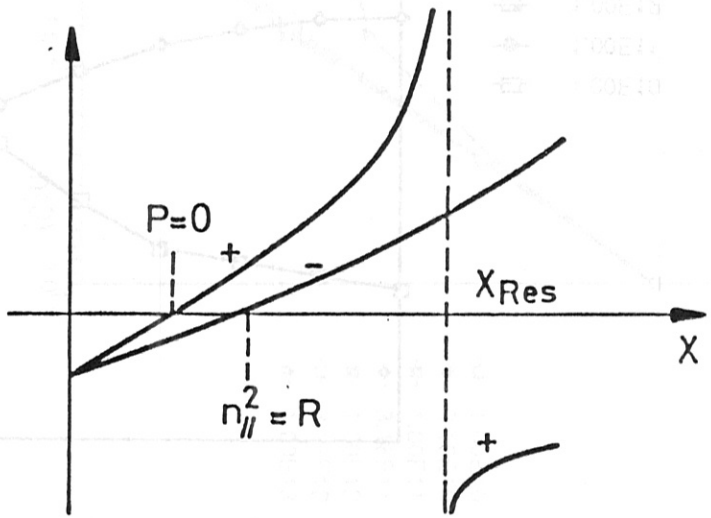

d) $y^2 < 1/2 ; \; n_{//}^2 > 1/(1-y^2) = 1 + (\omega_{Pe}^2/\Omega_{ce}^2)_{Res}$

FIG. 6

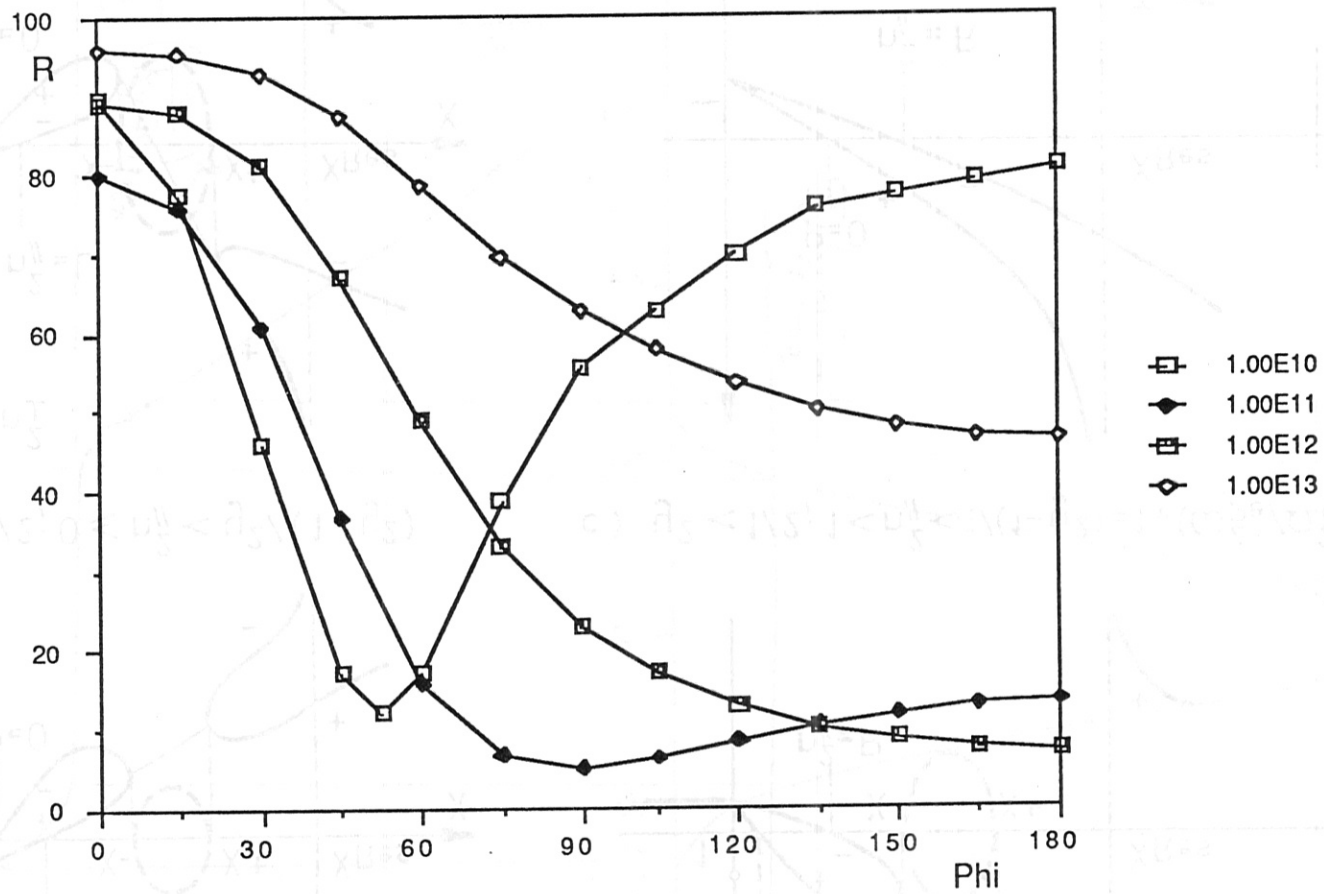
100
R
80
60
40
20
0
0
30
60
90
120
150
180
Phi
1.00E10
1.00E11
1.00E12
1.00E13

FIG. 7

Phase = 90

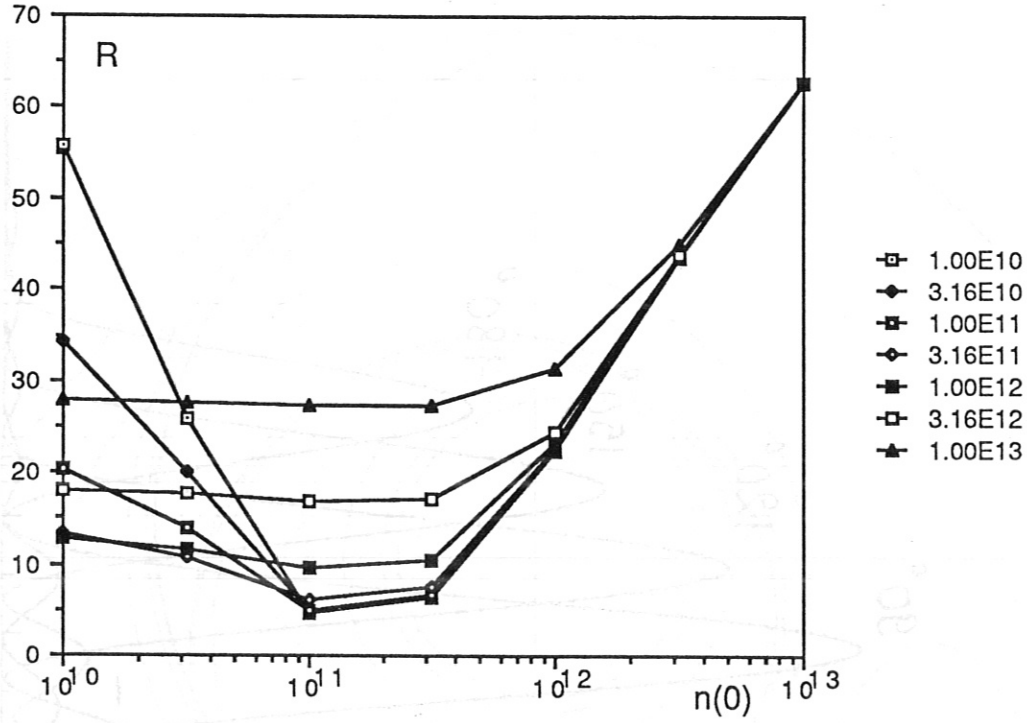

Phase = 180

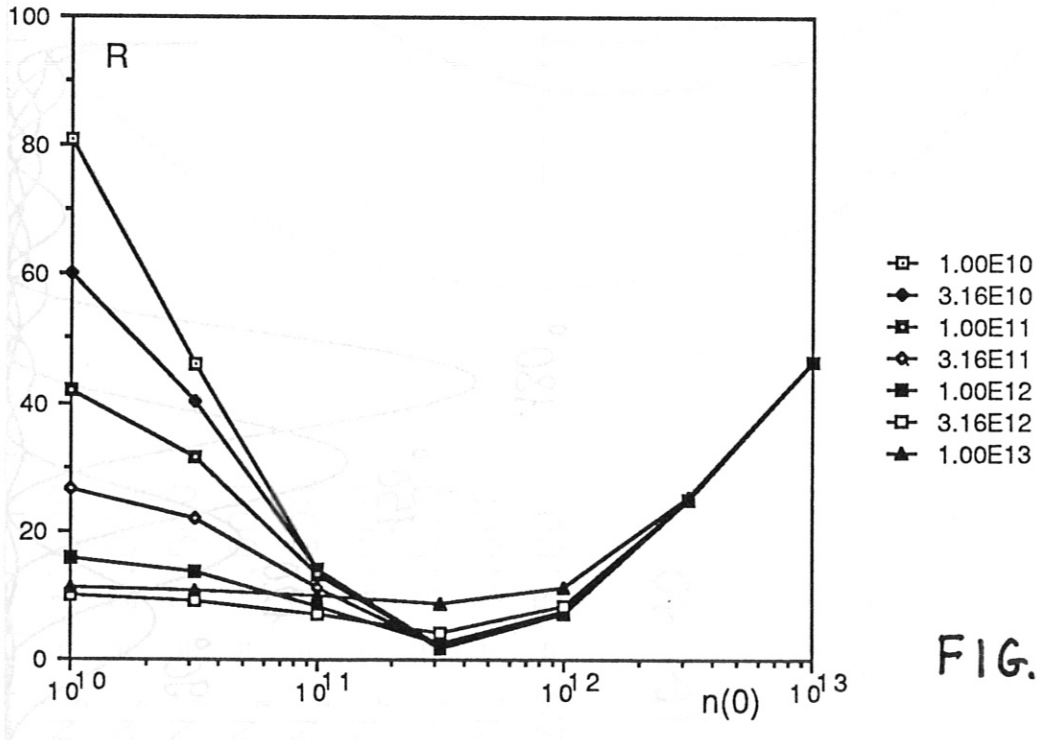

FIG. 8

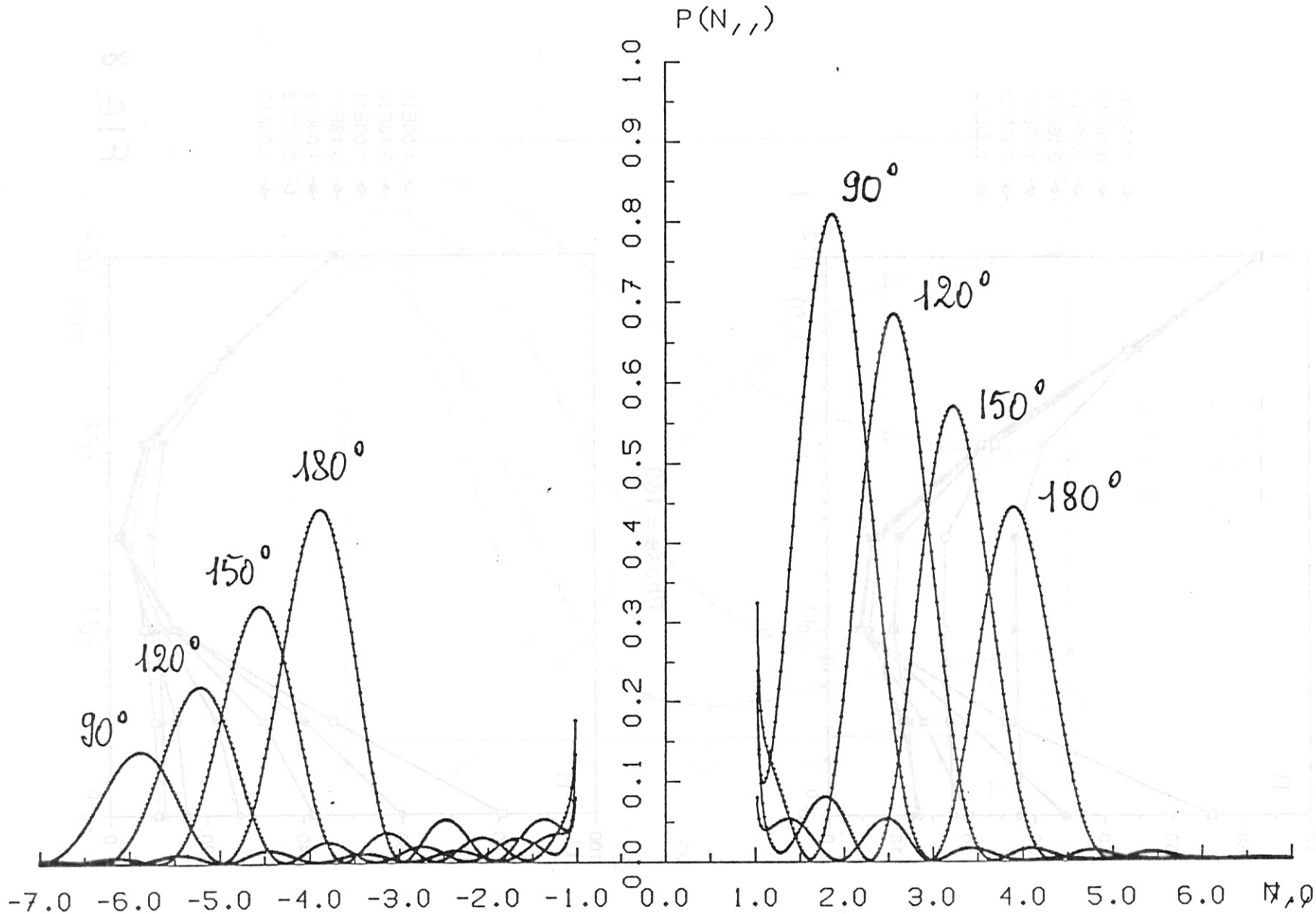
P(N,,)
1.0
0.9
0.8
0.7
0.6
0.5
0.4
0.3
0.2
0.1
0
90°
120°
150°
180°
90°
120°
150°
180°
-7.0 -6.0 -5.0 -4.0 -3.0 -2.0 -1.0 0.0 1.0 2.0 3.0 4.0 5.0 6.0
N,0

FIG. 9

1 – N_z = 1.500
N_z = 2.000
N_z = 2.500
N_z = 3.000
N_z = 3.500
N_z = 4.000
N_z = 4.500
8 – N_z = 5.000
ΔS = 5.00

FIG. 10

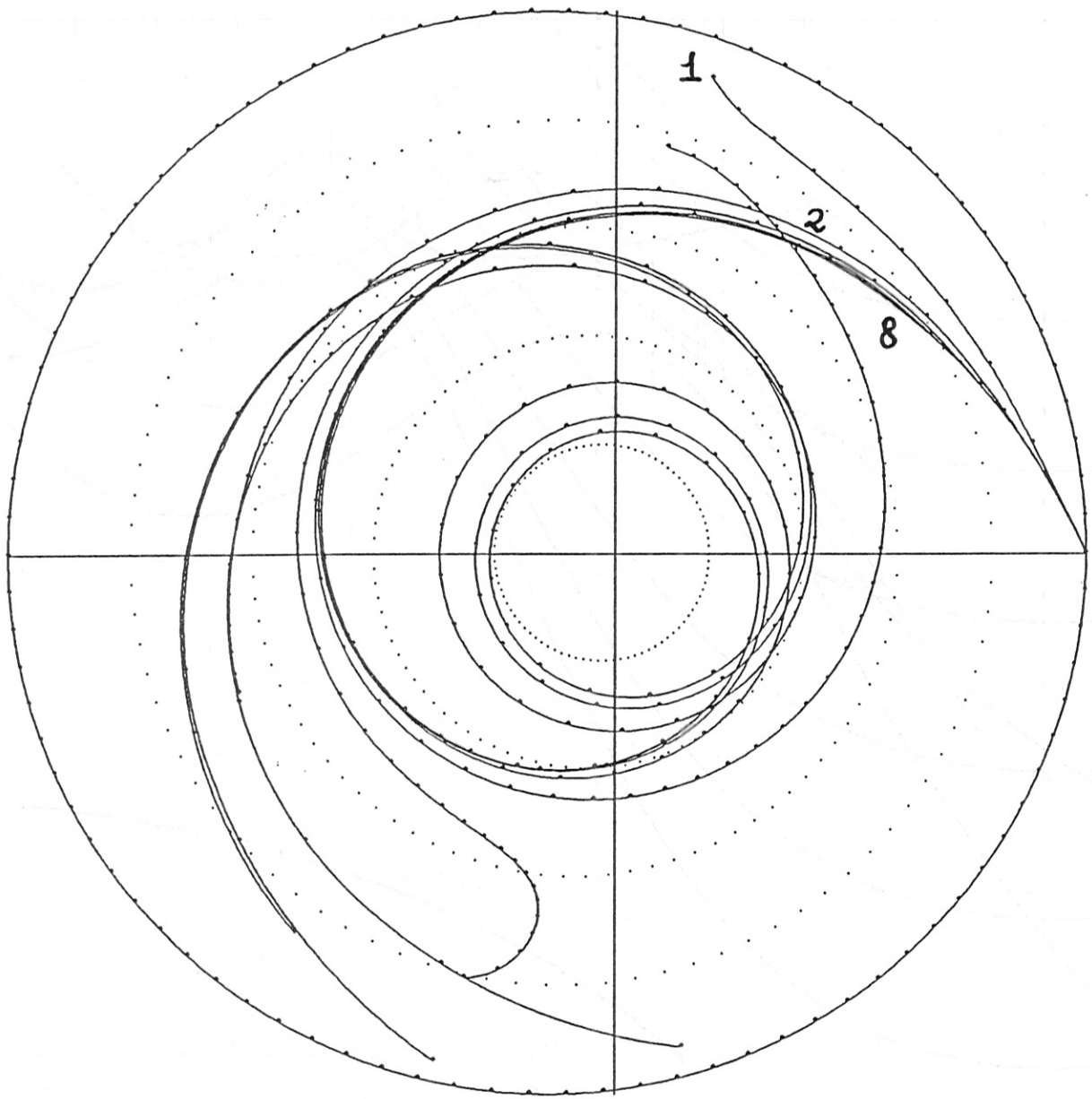

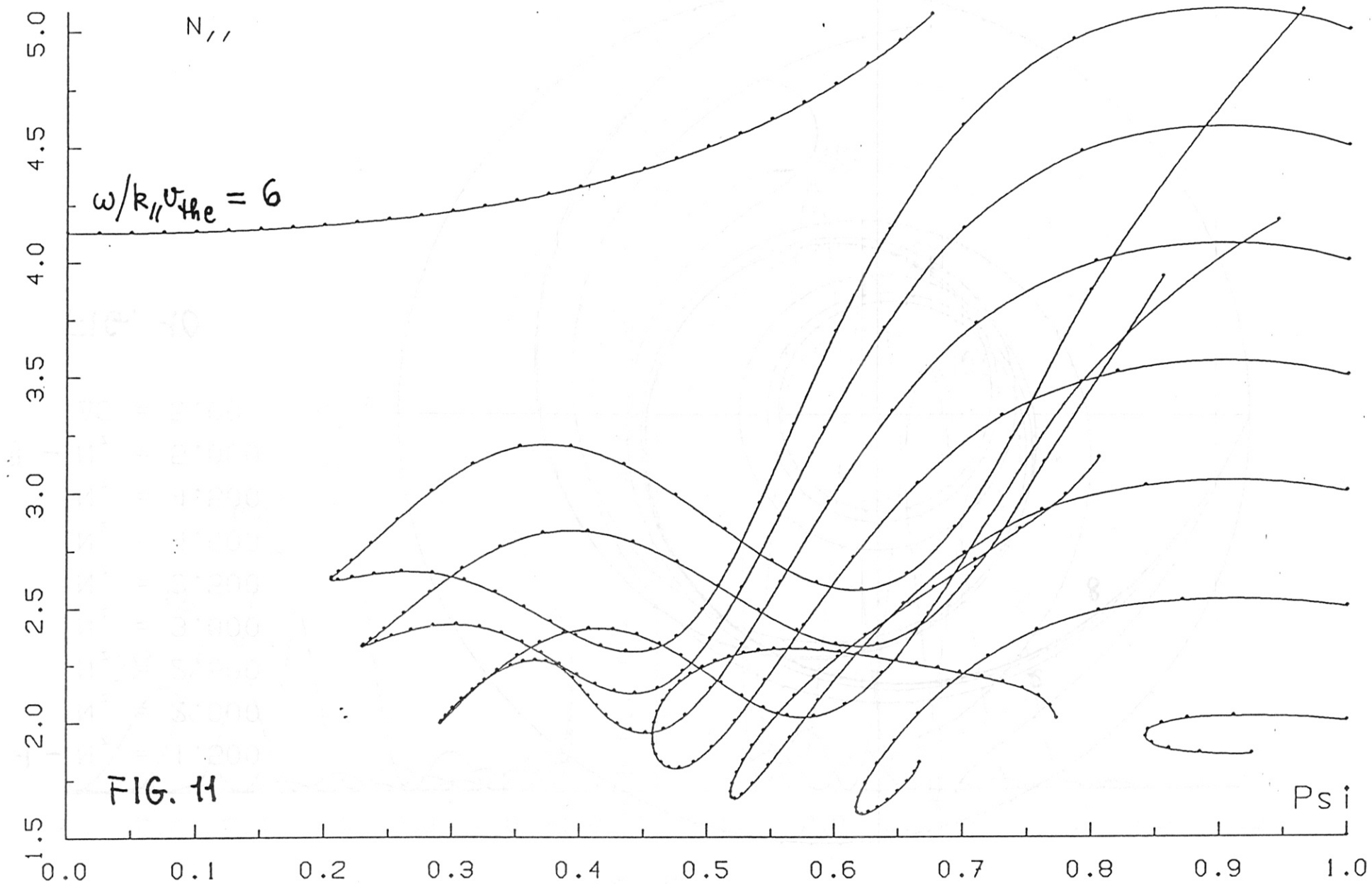
N,,
$\omega/k_{\parallel}v_{the} = 6$
5.0
4.5
4.0
3.5
3.0
2.5
2.0
1.5
0.0
0.1
0.2
0.3
0.4
0.5
0.6
0.7
0.8
0.9
1.0
Psi

FIG. 11

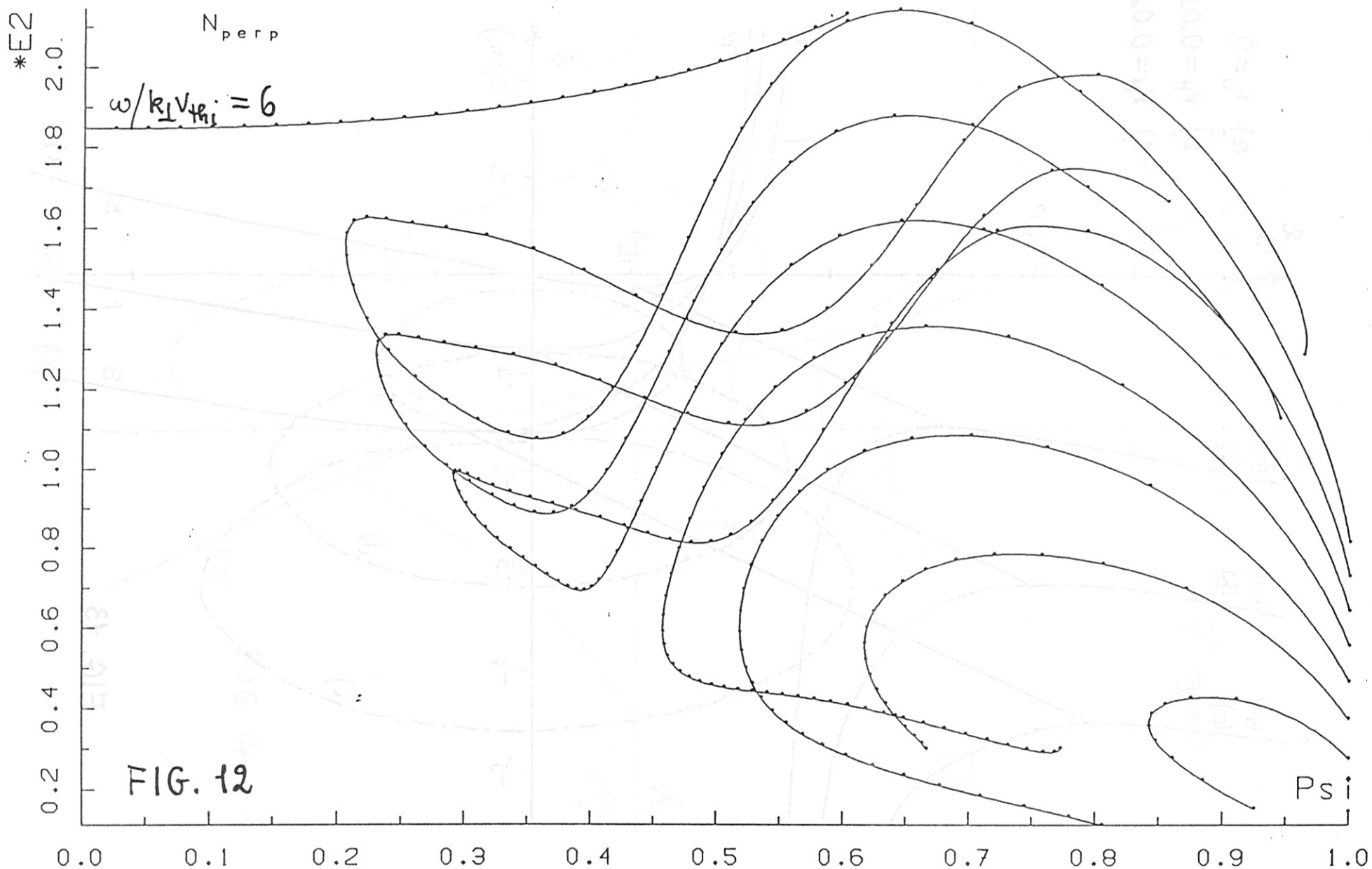
*E2
N_{perp}
$\omega/k_\perp v_{th_i} = 6$
0.2
0.4
0.6
0.8
1.0
1.2
1.4
1.6
1.8
2.0
0.0
0.1
0.2
0.3
0.4
0.5
0.6
0.7
0.8
0.9
1.0
Psi

FIG. 12

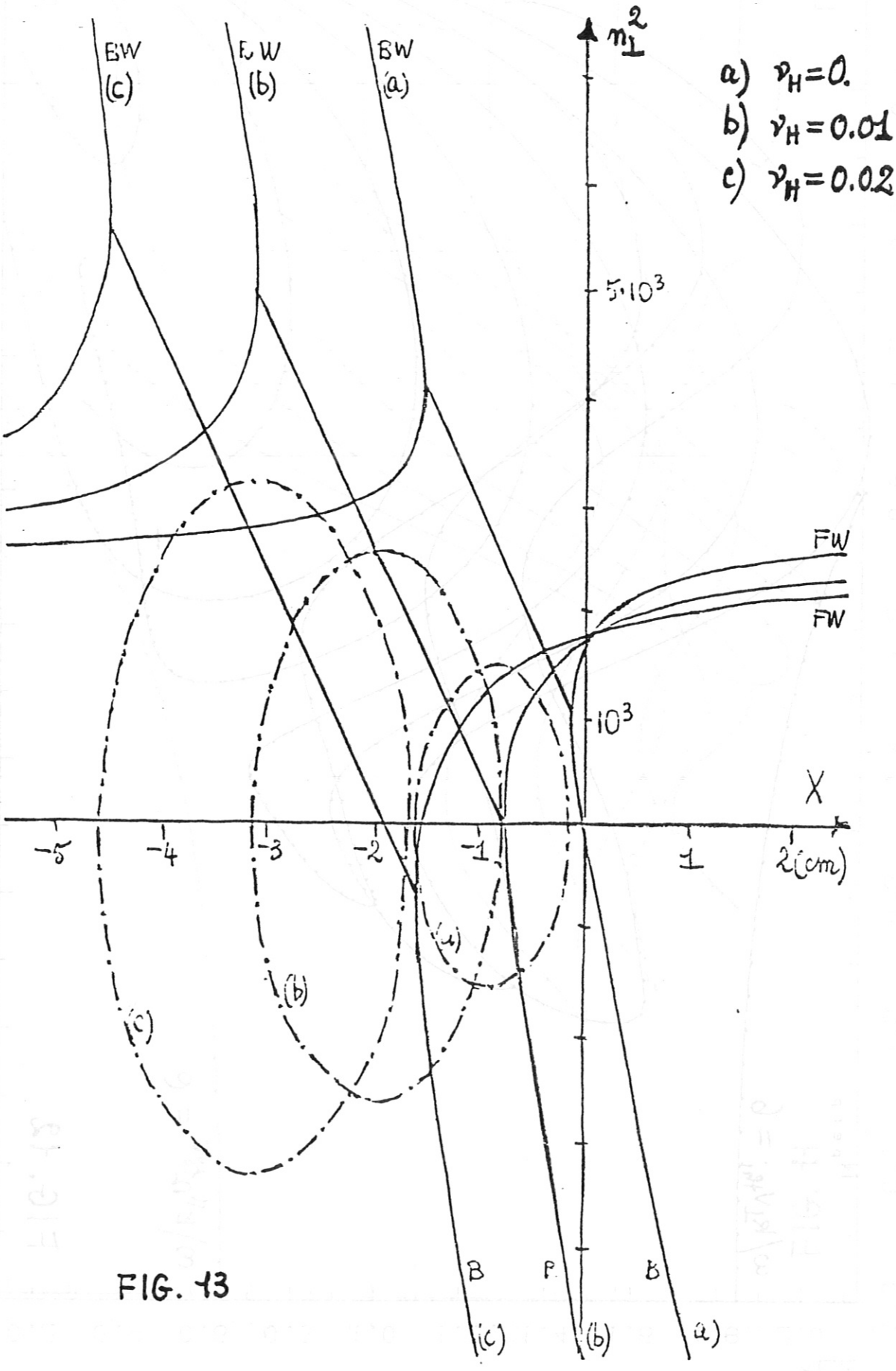
BW
(c)
BW
(b)
BW
(a)
$n_\perp^2$
a) $\nu_H = 0.$
b) $\nu_H = 0.01$
c) $\nu_H = 0.02$
$5 \cdot 10^3$
FW
FW
10^3
X
-5
-4
-3
-2
-1
1
2(cm)
(c)
(b)
(a)
B
P
B
(c)
(b)
a)

FIG. 13

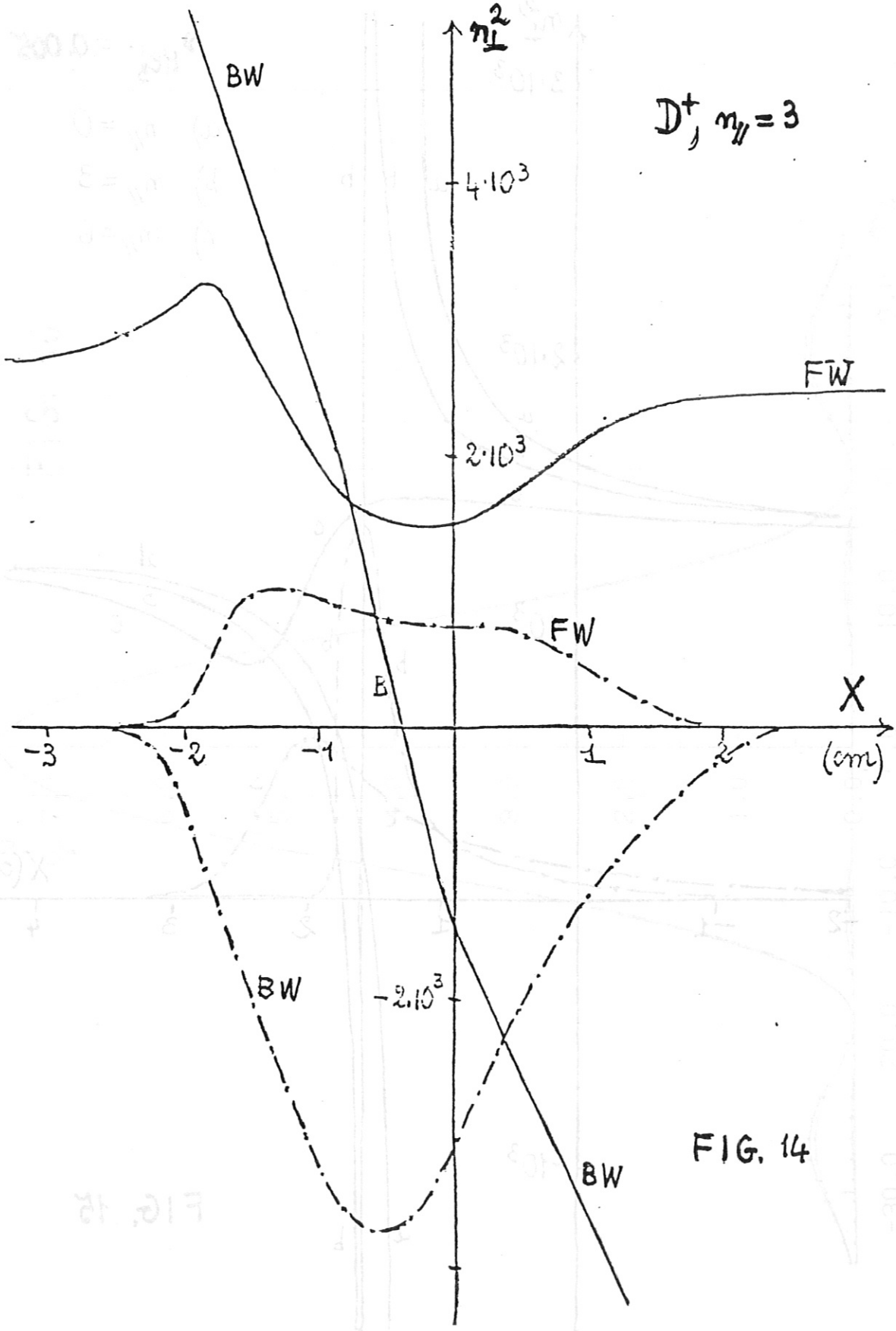
$n_\perp^2$
D^+, $n_{//} = 3$
BW
$4 \cdot 10^3$
FW
$2 \cdot 10^3$
FW
B
X
-3
-2
-1
1
2
(cm)
BW
$-2 \cdot 10^3$
BW

FIG. 14

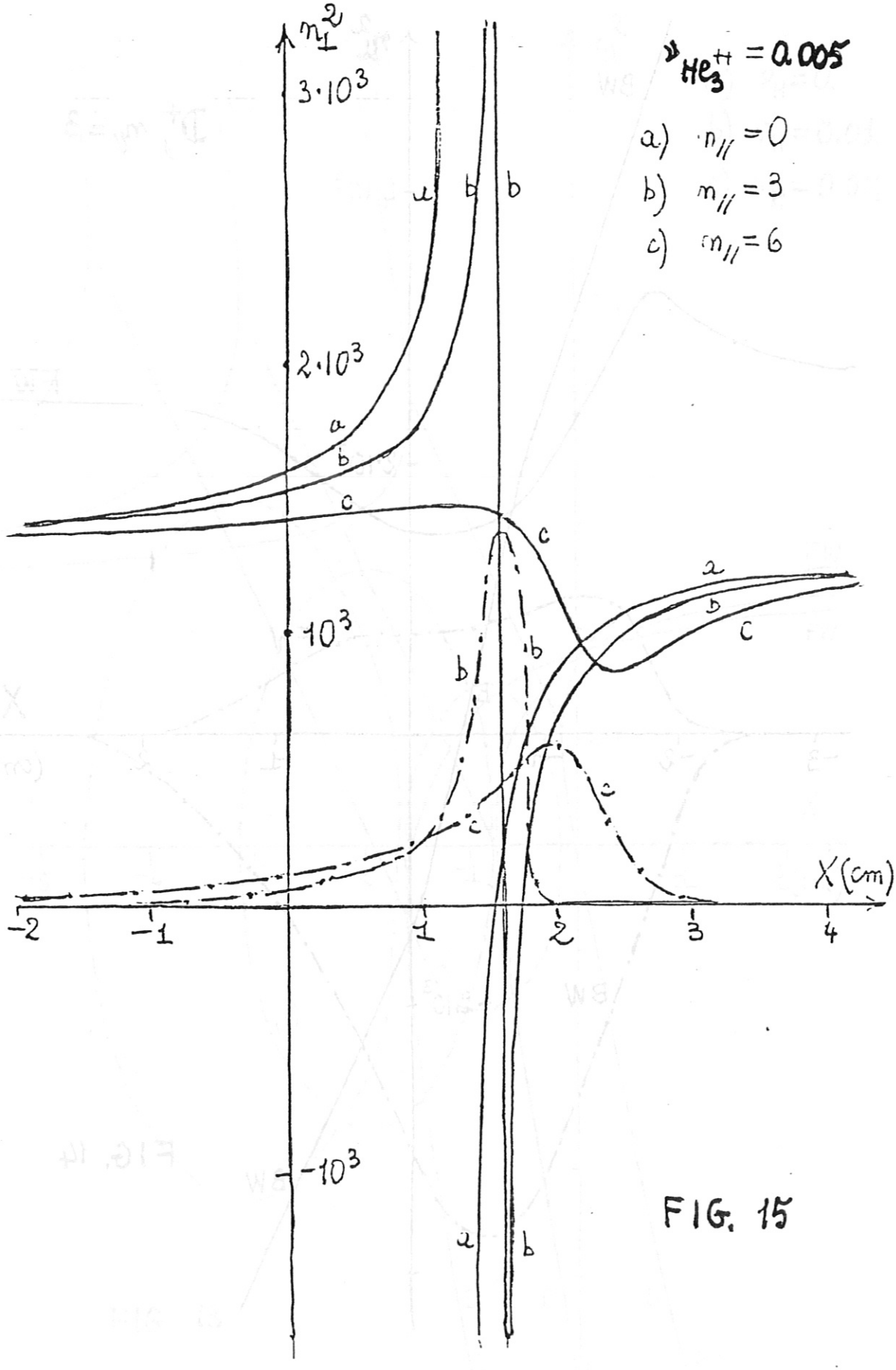
$n_\perp^2$
$3 \cdot 10^3$
$2 \cdot 10^3$
10^3
-10^3
$\eta_{He_3^{++}} = 0.005$
a) $n_{//} = 0$
b) $n_{//} = 3$
c) $n_{//} = 6$
X (cm)
-2
-1
1
2
3
4

FIG. 15

FIG. 16

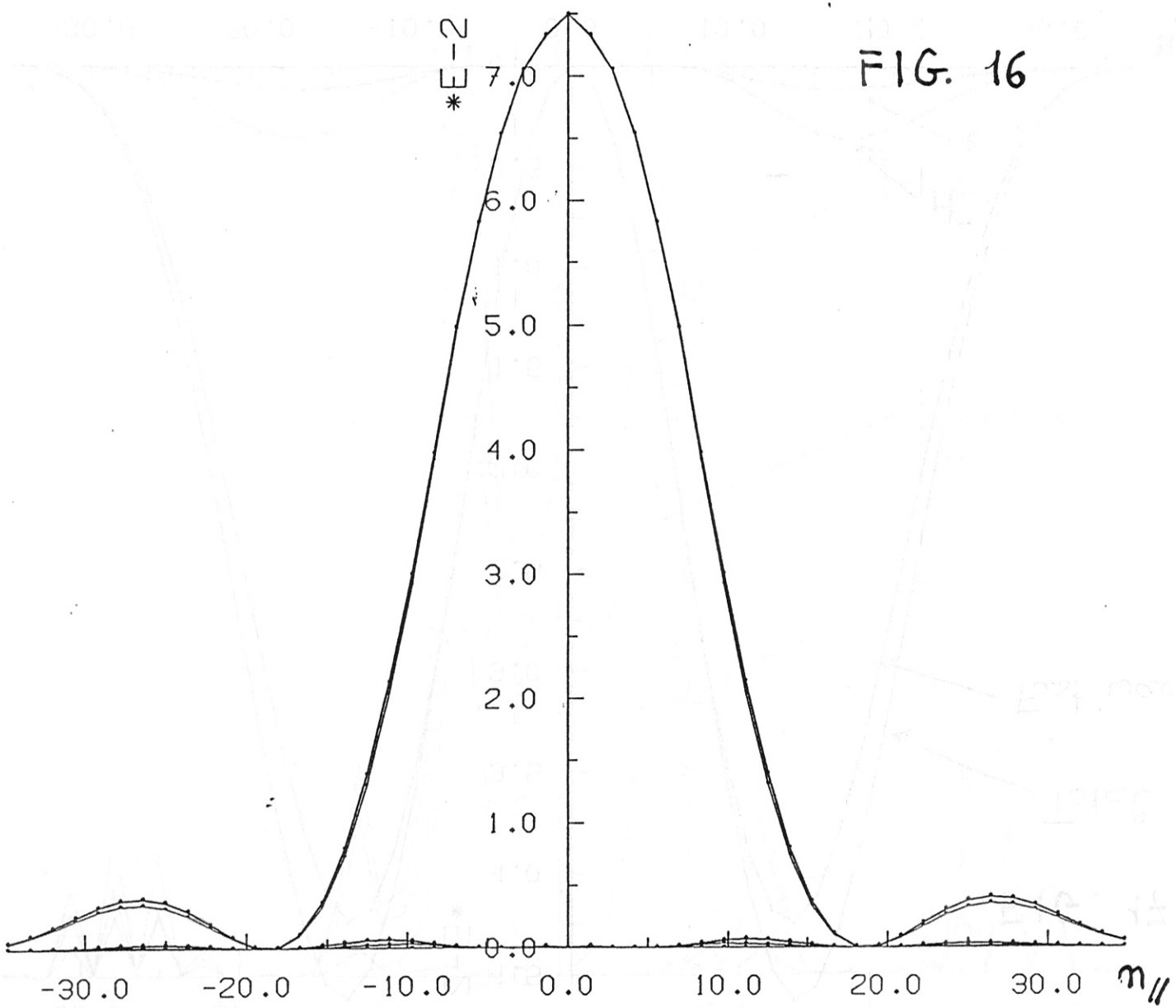

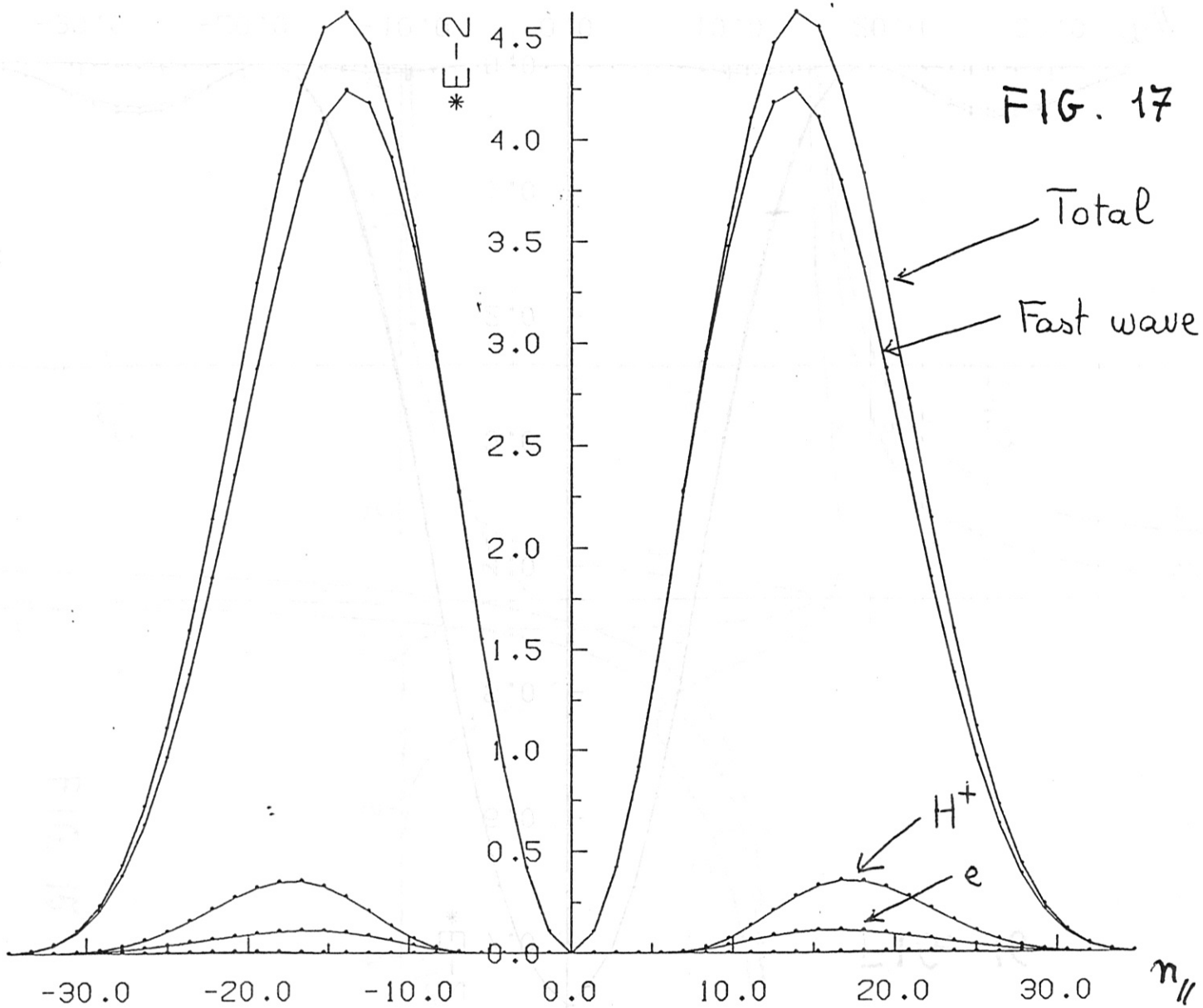
E-2 *
4.5
4.0
3.5
3.0
2.5
2.0
1.5
1.0
0.5
0.0
-30.0
-20.0
-10.0
0.0
10.0
20.0
30.0
$n_{//}$
Total
Fast wave
H^+
e

FIG. 17

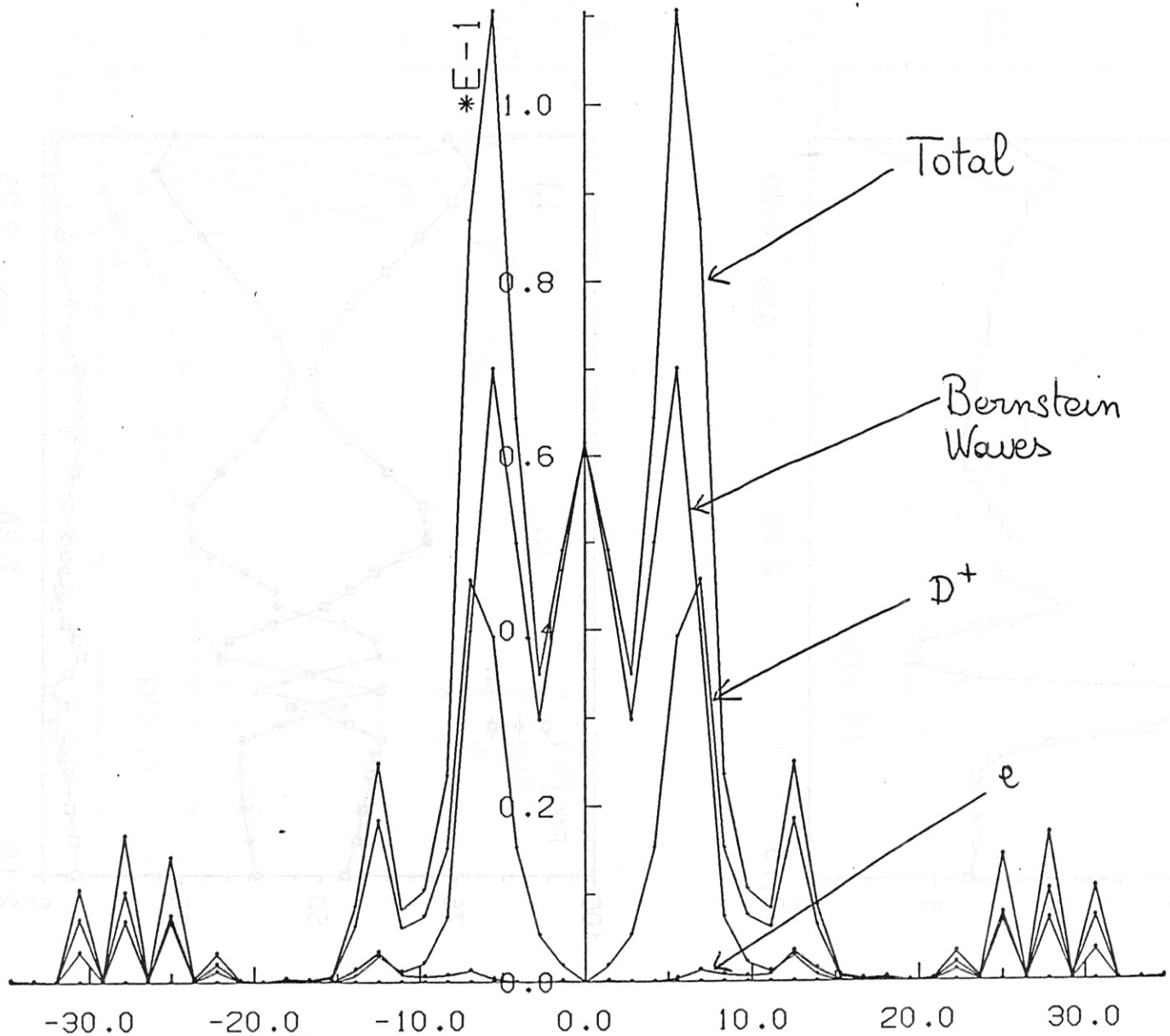
*E-1
1.0
0.8
0.6
0.4
0.2
0.0
-30.0
-20.0
-10.0
0.0
10.0
20.0
30.0
Total
Bernstein Waves
D+
e

FIG. 18

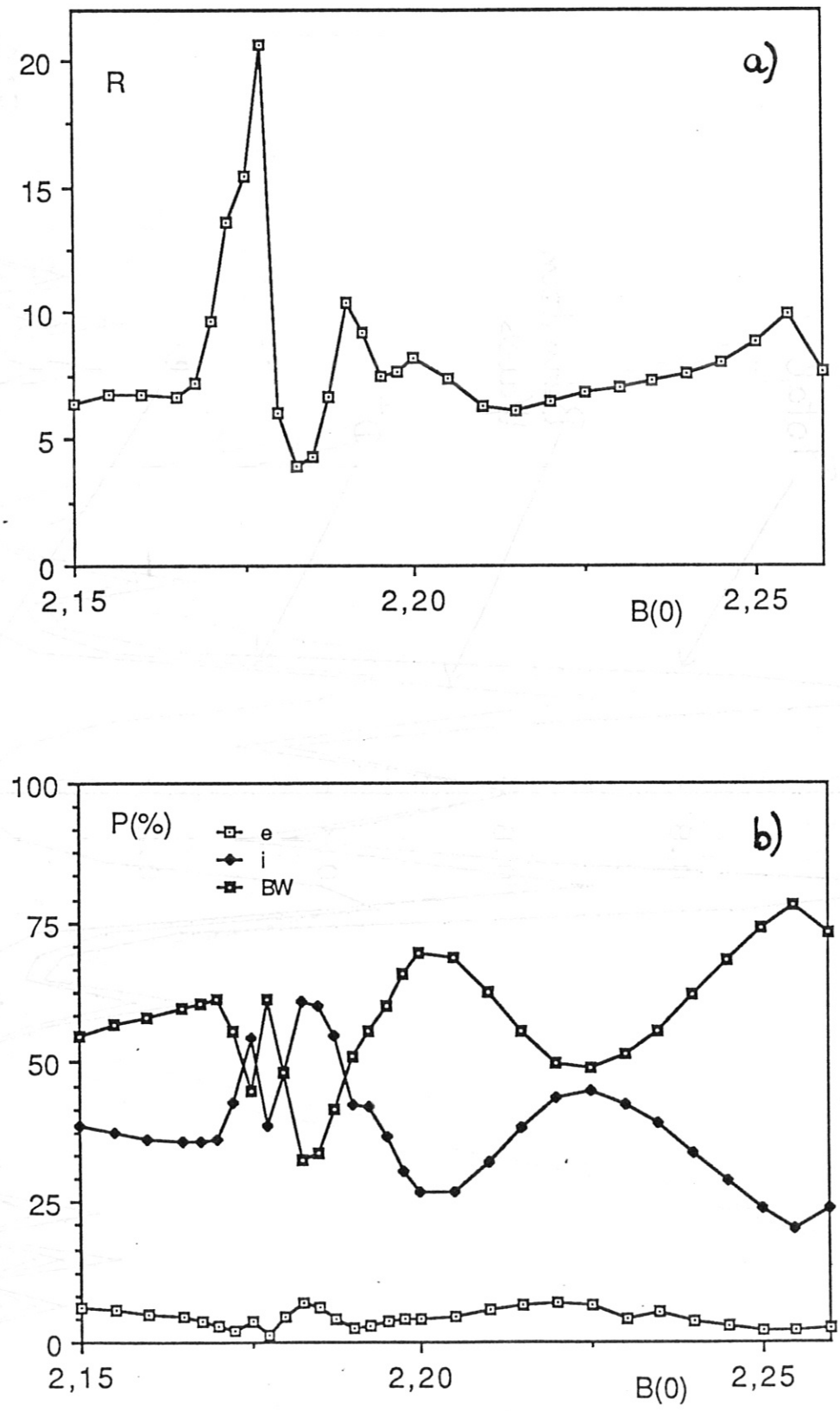

FIG. 19

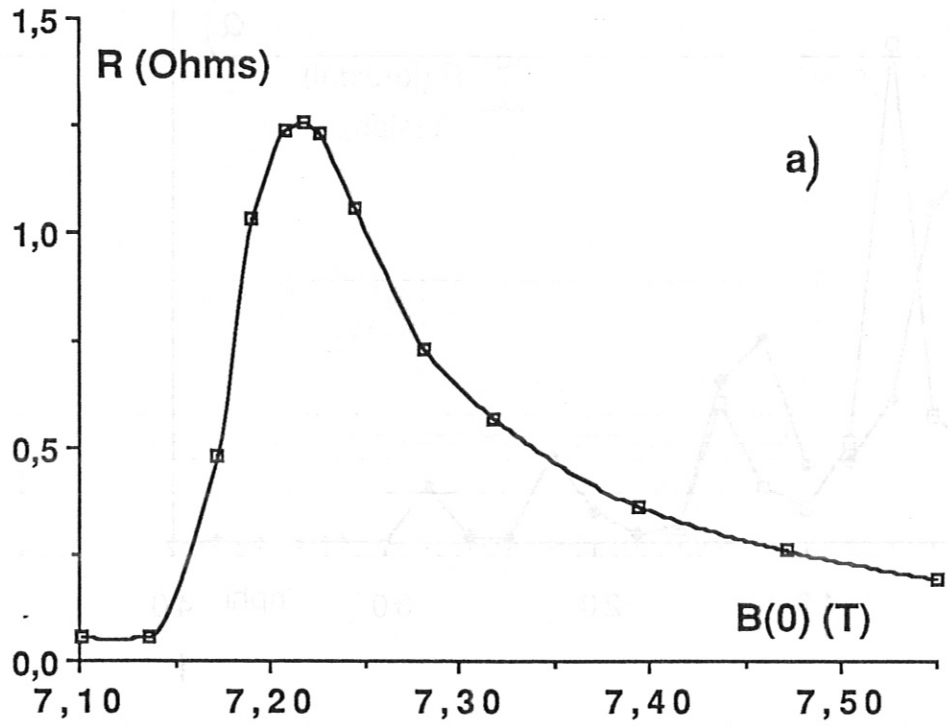
1,5
R (Ohms)
a)
1,0
0,5
0,0
B(0) (T)
7,10
7,20
7,30
7,40
7,50

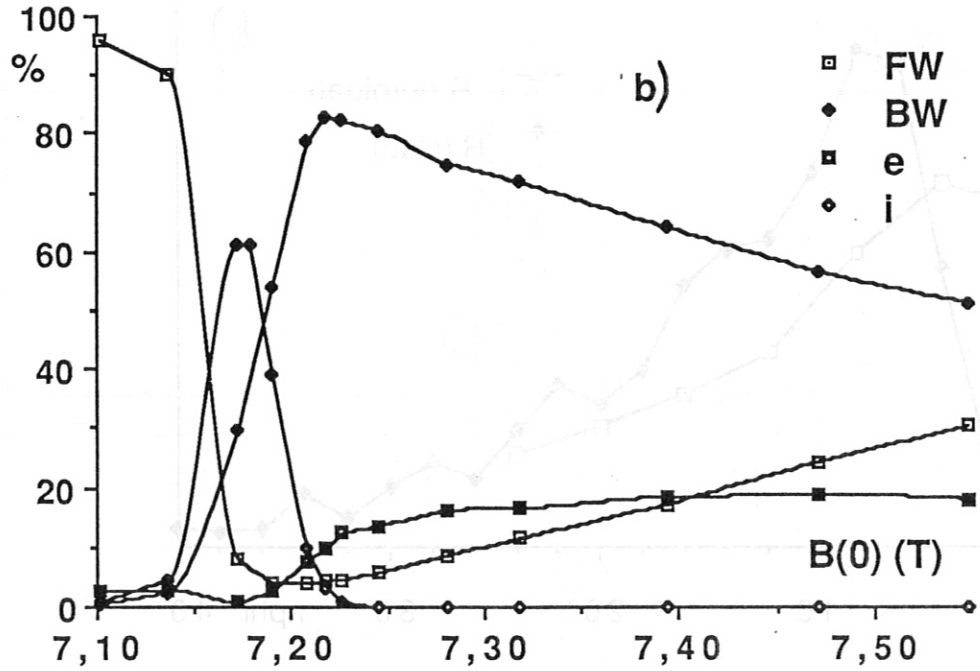
100
%
b)
FW
BW
e
i
80
60
40
20
0
B(0) (T)
7,10
7,20
7,30
7,40
7,50

FIG. 20

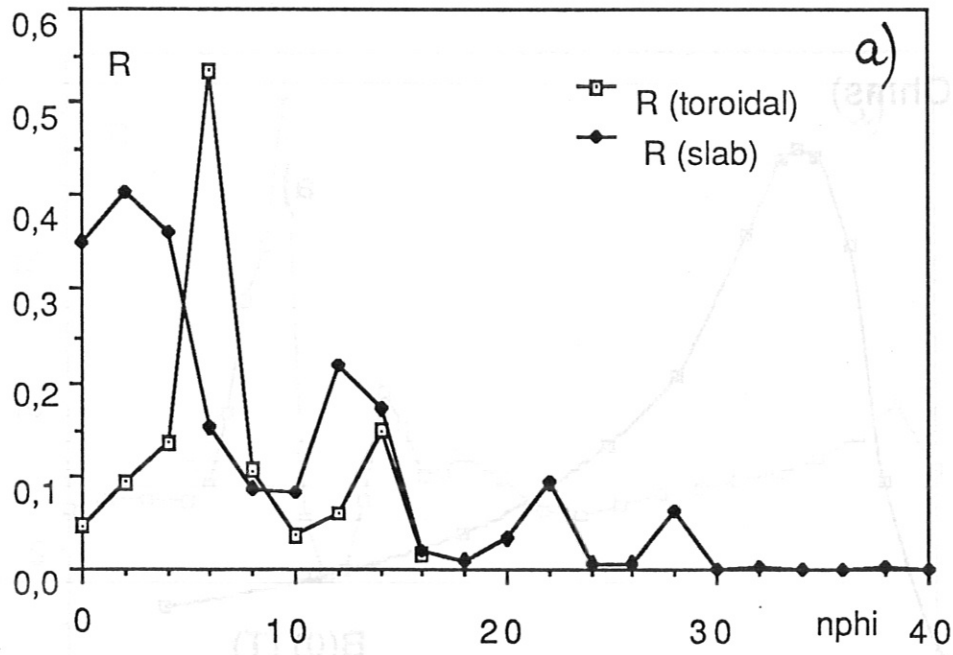
a)
R
R (toroidal)
R (slab)
0,6
0,5
0,4
0,3
0,2
0,1
0,0
0
10
20
30
nphi
40

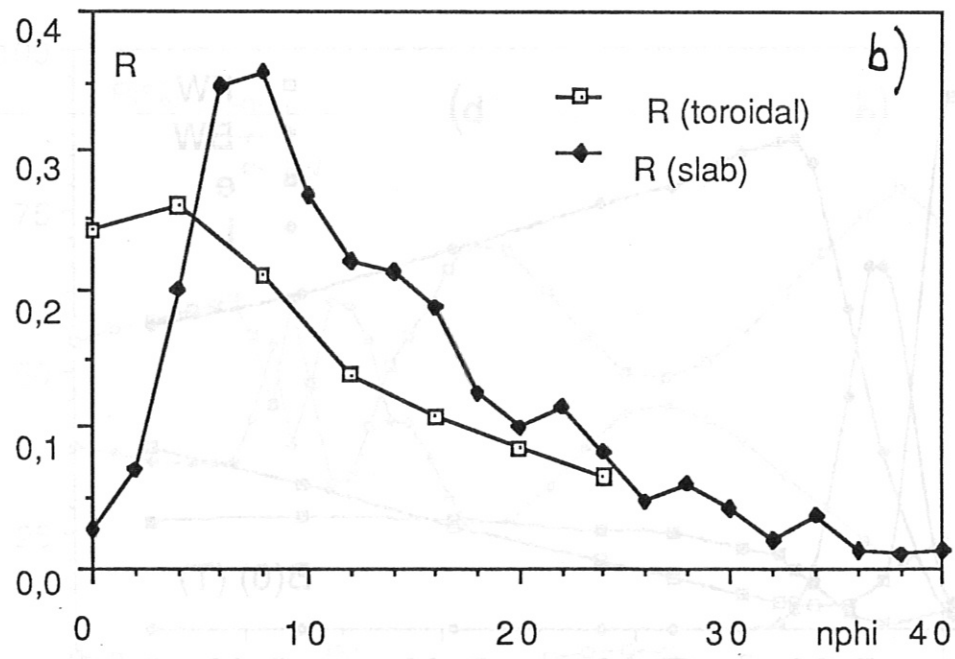
b)
R
R (toroidal)
R (slab)
0,4
0,3
0,2
0,1
0,0
0
10
20
30
nphi
40

FIG. 21

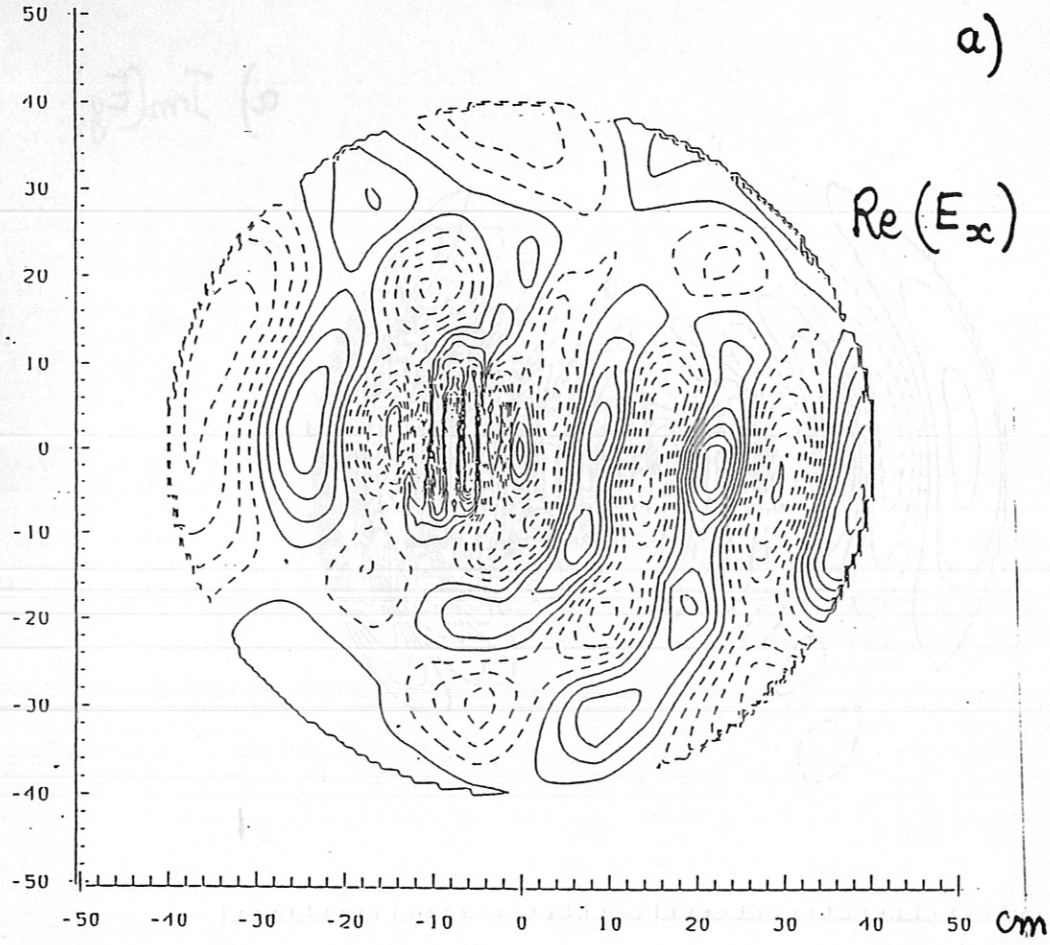
a)
Re (E_x)
50
40
30
20
10
0
-10
-20
-30
-40
-50
-50 -40 -30 -20 -10 0 10 20 30 40 50 cm

FIG. 22

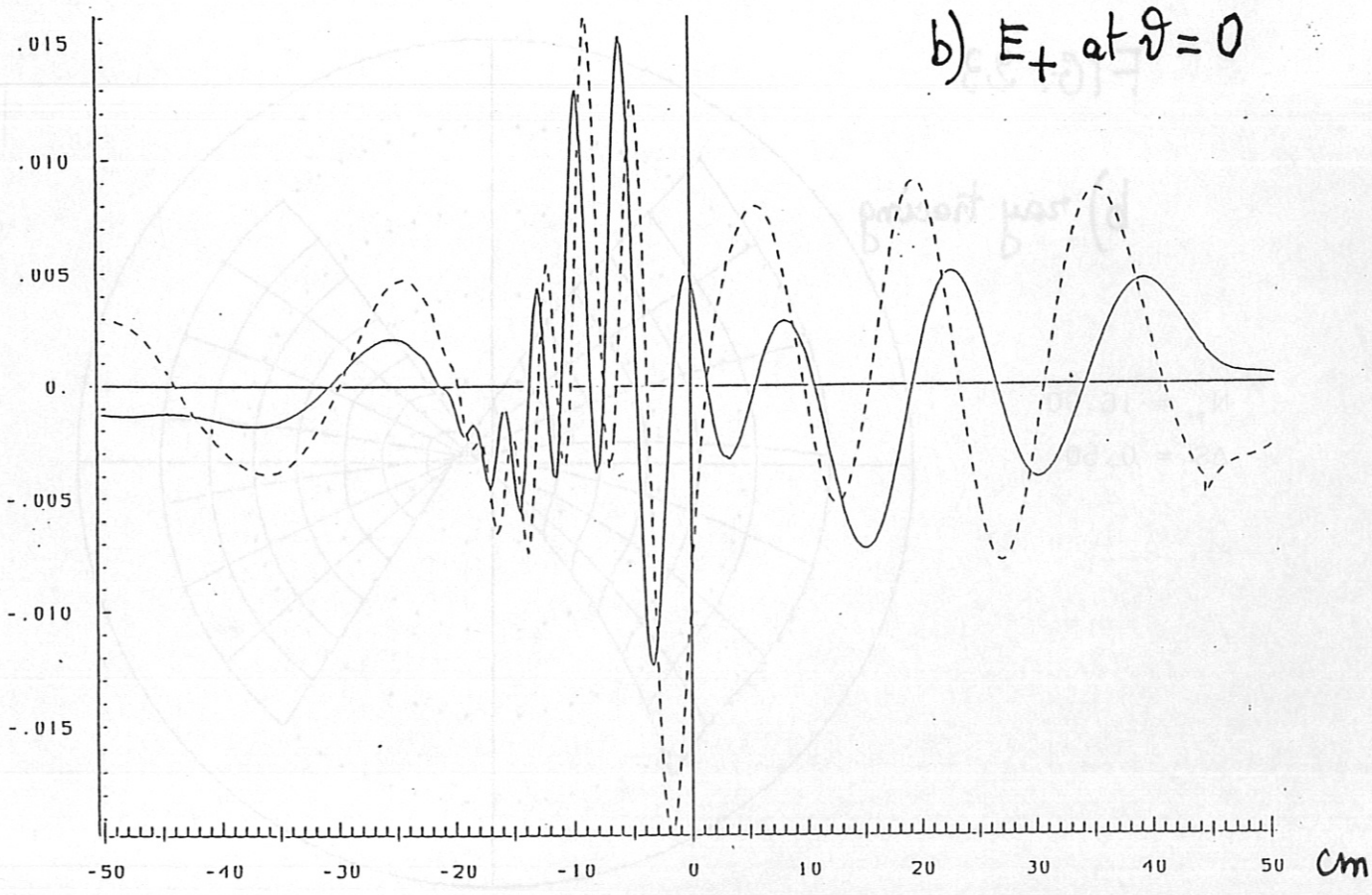
b) E+ at ϑ = 0
.015
.010
.005
0.
-.005
-.010
-.015
-50 -40 -30 -20 -10 0 10 20 30 40 50 cm

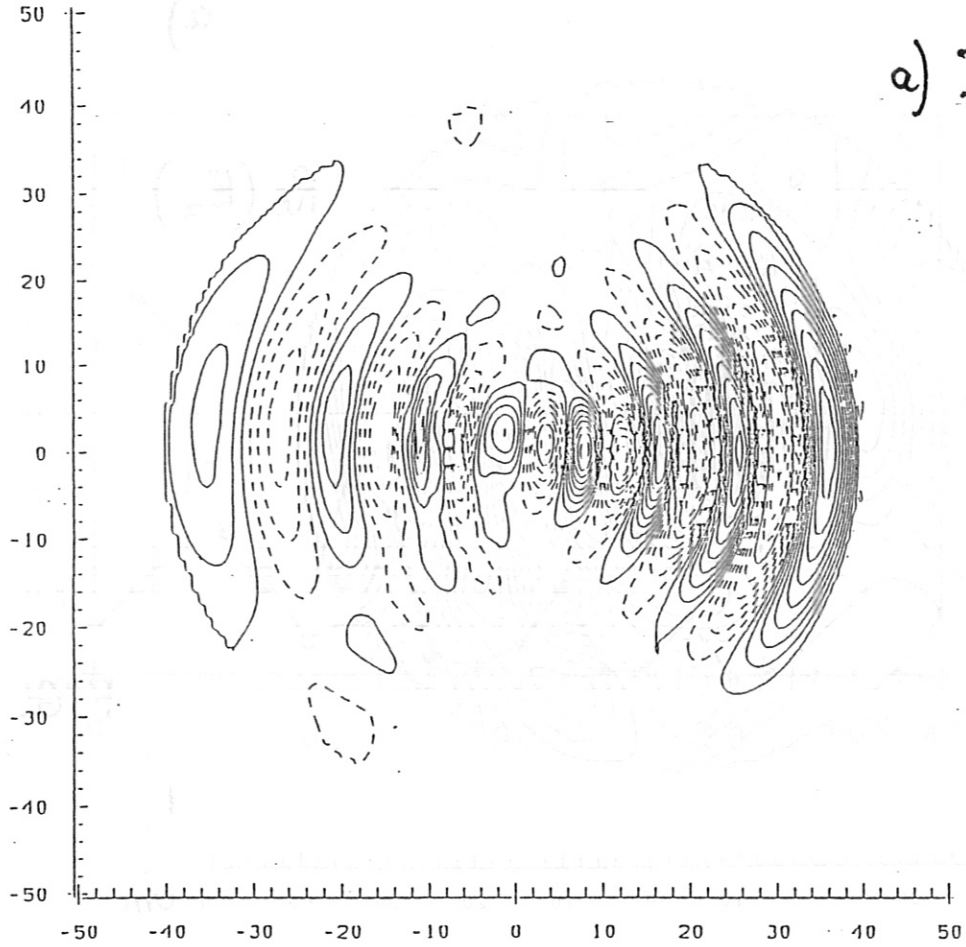

FIG. 23

b) ray tracing

N_φ = 16.00

ΔS = 0.50